Chern invariants for continuous media

Mário G. Silveirinha[*]

University of Coimbra, Department of Electrical Engineering – Instituto de Telecomunicações, Portugal
(Received 1 August 2015; revised manuscript received 2 September 2015; published 30 September 2015)

Here, we formally develop theoretical methods to topologically classify a wide class of bianisotropic continuous media. It is shown that for continuous media, the underlying wave vector space may be regarded as the Riemann sphere. We derive sufficient conditions that ensure that the pseudo-Hamiltonian that describes the electrodynamics of the continuous material is well behaved so that the Chern numbers are integers. Our theory brings the powerful ideas of topological photonics to a wide range of electromagnetic waveguides and platforms with no intrinsic periodicity and sheds light over the emergence of edge states at the interfaces between topologically inequivalent continuous media.

PACS number(s): 42.70.Qs, 03.65.Vf, 78.67.Pt, 78.20.Ls

I. INTRODUCTION

The photonic crystal concept was introduced in 1987 in connection with a proposal to inhibit the spontaneous emission and thereby enhance the performance of semiconductor lasers [1]. Starting with this already distant pioneering study, photonic crystals have revolutionized light-based technologies and laid the foundations for future integrated photonic platforms fully operated with light waves [2,3]. The light propagation in photonic crystals is dictated by a band structure that comprises all the relevant information about the allowed photonic states [2]. The general approach to control the flow of light in these artificial materials relies on the so-called band structure engineering. In particular, the unit cell of a photonic crystal determines the light dispersion, i.e., the relation between frequency and the wave vector, and the polarization of the light waves. In most applications, one is interested in the properties of the band structure in a narrow frequency range. The unprecedented control over the photonic band structure unveiled a plethora of new phenomena [4,5], and, in particular, it lead to the development of electromagnetic metamaterials [6].

Surprisingly, it was recently discovered that the light propagation in photonic crystals may also depend on the *global* properties of the band structure, i.e., on some *topological* characteristics that depend on the inner fabric of all the eigenstates over a wide range of frequencies [7–9] and on the manner that they are mutually entangled. It has been suggested that topological invariants may have revolutionary applications in future photonic platforms immune to disorder and imperfections and may allow for new paradigms for a topologically protected transport of optical energy [10–16].

The analogies between electronics and photonics are at the heart of the foundation of photonic crystals [1]. The study of the topological properties of photonic crystals was also inspired by such analogies [7,8]. Topology is a branch of mathematics related to the qualitative geometrical properties of objects. The topological classification of surfaces is a well-developed subject [17]. A recurring example is that a torus and a sphere are topologically inequivalent because they cannot be transformed one into the other with a continuous transformation. Different topologies are mathematically classified by integer numbers, designated by topological invariants, which are quantities unaffected by continuous deformations of the system [9,17]. The emergence of topological concepts in solid-state physics dates back to 1982 with the proof that the Hall conductance of a two-dimensional periodic potential is precisely quantized [18,19]. The integer number that defines the conductivity is known as the Chern number and is determined by all the filled electronic bands. Thus, the Chern number depends on the *global* properties of the band structure. An important development occurred some years ago when Haldane and Raghu suggested that a photonic crystal with a broken time-reversal symmetry (e.g., in a periodic array of biased ferrite disks) may be characterized by nontrivial Chern numbers [7,8]. It was proven that the nontrivial topological nature of these structures may imply the existence of one-way topologically protected chiral edge states immune to disorder and imperfections. These ideas were verified in an experiment [12] that confirmed that the edge states can travel in a single direction and are largely insensitive to the presence of large scatterers. Indeed, the edge states route around any obstacles placed in their path, with no reflections, because of the inexistence of backwards-propagating edge states [12]. Thus, the topological nature of chiral edge states makes the wave propagation impervious to imperfections.

Recently, the field of topological photonics received a further boost of interest with the discovery of topological photonic insulators, which are essentially photonic crystals that may support topologically protected edge states even though the time-reversal symmetry is unbroken [20,21]. This is an advancement worth noting because it enables us to realize chiral edge states, relying on conventional dielectrics and metals [21], without the need for the less common nonreciprocal materials. Different from magneto-optic photonic crystals, in a topological photonic insulator the edge states are bidirectional. Yet, they have intrinsic chiral-type properties that make them largely immune to back scattering [20,21]. The concept of a topological insulator originally emerged in condensed matter physics [22,23].

The usual topological classification of photonic crystals explores the fact that these structures are periodic [7–9]. The periodicity is essential for technical reasons. Indeed, to ensure that the Chern number is an integer, it is necessary

---

[*]Author to whom correspondence should be addressed: mario.silveirinha@co.it.pt

that the underlying wave vector space is a closed surface with no boundary [23]. In a photonic crystal, the relevant space is the Brillouin zone, which is equivalent to a torus. It would be interesting to extend the topological classification of photonic crystals to continuous electromagnetic media, e.g., to metamaterials modeled by some effective parameters. Indeed, the electrodynamics of continuous systems is much simpler than that of periodic structures, and this simplicity may lead to important physical insights and a deeper understanding of topological photonics. Similar to photonics crystals, due to the frequency dispersion of the material response, continuous media are also characterized by an intricate band structure. However, unlike in periodic structures, for continuous media the natural wave vector space is an unbounded open region (the Euclidean space). Thus, the topological classification of continuous media seems unfeasible. Yet, given that the Chern numbers are integral for periodic systems, one might be tempted to conclude that the homogeneous systems have the same property because of two possible paths. In the first, the period of a periodic system is taken to infinity. In the second, a periodic system with inclusions is considered, and the difference between the materials in the inclusions and in the background is made to tend to zero. Unfortunately, both paths are misleading. For the first case, the explanation is that when the period approaches infinity, the Brillouin zone (a torus) collapses into a point (in the limit where the period is exactly infinity). Hence, the final wave vector space (when the period is precisely infinity) is not a closed surface with no boundary, as required by the Chern theorem. As to the second case, the problem is that in the continuous limit, two generic wave vectors that differ by a primitive reciprocal lattice vector (let us say $\mathbf{k}$ and $\mathbf{k} + \mathbf{G}$) are not equivalent, different from what happens in the periodic case. Indeed, in the periodic case, it is possible to link the envelopes of the eigenfunctions as $\mathbf{f}_{n\mathbf{k}+\mathbf{G}} = \mathbf{f}_{n\mathbf{k}} e^{i\mathbf{G}\cdot\mathbf{r}}$ (a Gauge transformation), whereas in the continuous limit $\mathbf{f}_{n\mathbf{k}}$ and $\mathbf{f}_{n\mathbf{k}+\mathbf{G}}$ are unrelated. Due to this reason, in the continuous limit the Brillouin zone is not equivalent to a torus.

It is demonstrated in this paper that it is possible to overcome these technical difficulties and to calculate the Chern invariants of a wide class of continuous bianisotropic electromagnetic media described by an effective material response. The key ingredient is to map the unbounded wave vector space into the Riemann sphere. We derive general conditions that guarantee that the pseudo-Hamiltonian associated with a given dispersive material response is sufficiently well behaved over the Riemann sphere so that the Chern numbers are integers. We illustrate the application of the theory with several physically intuitive examples and connect the nontrivial topology of bulk continuous media with the emergence of edge states.

This paper is organized as follows. In Sec. II we extend the theory of Raghu and Haldane [8] to general bianisotropic spatially dispersive media and explain how the Berry potential can be determined from the continuous medium band structure. Next, in Sec. III, it is shown that the wave vector space associated with continuous media may be identified with the Riemann sphere. We derive a wide class of bianisotropic material responses for which the associated pseudo-Hamiltonian is sufficiently well behaved so that the Chern numbers are integers. In Sec. IV, the developed theory is applied to

characterize the Chern invariants of a magneto-optic material. The correlation between the nontrivial topology of the continuous medium and the emergence of edge states is discussed. The conclusions are drawn in Sec. V.

II. THE BERRY POTENTIAL FOR DISPERSIVE LOSSLESS MEDIA

A. Continuous electromagnetic media

In this paper, we are interested in dispersive lossless media, whose electrodynamics in the time domain is described in a compact manner by

$$\hat{N} \cdot \mathbf{f} = i \left[\frac{\partial \mathbf{g}}{\partial t} + \mathbf{j} \right], \tag{1}$$

where $\mathbf{f} = (\mathbf{E} \quad \mathbf{H})^T$, $\mathbf{g} = (\mathbf{D} \quad \mathbf{B})^T$, and $\mathbf{j} = (\mathbf{j}_e \quad \mathbf{j}_m)^T$ are six-component vector fields, $\mathbf{E}, \mathbf{H}$ are the electric and magnetic fields, $\mathbf{D}, \mathbf{B}$ are the electric displacement and the induction fields, $\mathbf{j}_e, \mathbf{j}_m$ are the electric and magnetic current densities ($\mathbf{j}_m$ is included here only for the sake of completeness), and the superscript T denotes the transposition operation. The differential operator $\hat{N}$ stands for

$$\hat{N} = \begin{pmatrix} \mathbf{0} & i\nabla \times \mathbf{1}_{3\times 3} \\ -i\nabla \times \mathbf{1}_{3\times 3} & \mathbf{0} \end{pmatrix}, \tag{2}$$

where $\mathbf{1}_{3\times 3}$ is the identity tensor of dimension three. The $\mathbf{f}$ and $\mathbf{g}$ vector fields are linked in the spectral (frequency) domain by a material matrix $\mathbf{M}$ such that

$$\mathbf{g} = \mathbf{M} \cdot \mathbf{f}, \quad \text{with} \quad \mathbf{M} = \mathbf{M}(\omega, \mathbf{k}) = \begin{pmatrix} \varepsilon_0 \overline{\varepsilon} & \frac{1}{c}\overline{\xi} \\ \frac{1}{c}\overline{\zeta} & \mu_0 \overline{\mu} \end{pmatrix}. \tag{3}$$

In the above, $\omega = i\partial/\partial t$ is the frequency, $\mathbf{k} = -i\nabla$ is the wave vector, and the dimensionless tensors $\overline{\varepsilon}, \overline{\mu}, \overline{\xi}, \overline{\zeta}$ represent the permittivity tensor, the permeability tensor, and the magneto-electric coupling tensors, respectively [24]. Thus, we allow the material response to be bianisotropic [24,25], and it may depend both on the frequency and on the wave vector. Hence, the medium may be spatially dispersive, i.e., *nonlocal* [26,27], as opposed to conventional *local* media with $\mathbf{M} = \mathbf{M}(\omega)$. The reason for this assumption will be made clear in Sec. III. For future reference, we note that in a lossless medium the material matrix is required to be Hermitian for $(\omega, \mathbf{k})$ real-valued [25,28]

$$\mathbf{M}(\omega, \mathbf{k}) = \mathbf{M}^{\dagger}(\omega, \mathbf{k}), \tag{4}$$

where the superscript † denotes the conjugate transpose matrix. Moreover, the material matrix must also satisfy

$$\frac{\partial}{\partial \omega} [\omega \mathbf{M}(\omega, \mathbf{k})] > 0, \tag{5}$$

i.e., $\frac{\partial}{\partial \omega}[\omega \mathbf{M}(\omega, \mathbf{k})]$ must be a positive definite matrix. This property follows from the fact that the time-averaged stored energy density (W_{av}) in time-space harmonic regime ($\mathbf{f}(\mathbf{r}, t) = \text{Re}\{\mathbf{F}e^{-i\omega t} e^{i\mathbf{k}\cdot\mathbf{r}}\}$) is determined by the quadratic form $W_{\text{av}} = \frac{1}{4}\mathbf{F}^* \cdot \frac{\partial}{\partial \omega}[\omega \mathbf{M}(\omega, \mathbf{k})] \cdot \mathbf{F}$ and $W_{\text{av}} \geqslant 0$ [25]. Some particular cases of this formula are discussed in Refs. [26,27,29,30].

Finally, we note that because the electromagnetic fields are real-valued physical entities, the material matrix must satisfy

the reality condition [26,27],

$$\mathbf{M}(\omega,\mathbf{k}) = \mathbf{M}^*(-\omega,-\mathbf{k}), \tag{6}$$

where the superscript * stands for the conjugate operation.

B. Hermitian formulation in the time domain

In the absence of an external excitation ($\mathbf{j} = 0$), Maxwell's equations (1) become $\hat{N} \cdot \mathbf{f} = i\frac{\partial \mathbf{g}}{\partial t}$. When the material response is instantaneous (when $\mathbf{M}$ is independent of frequency), we get simply $\hat{H}_{cl} \cdot \mathbf{f} = i\frac{\partial \mathbf{f}}{\partial t}$ with $\hat{H}_{cl} = \mathbf{M}^{-1} \cdot \hat{N}$, which is similar to the Schrödinger equation with $\hbar = 1$. Notably, as discussed in Ref. [31], the operator $\hat{H}_{cl}$ is Hermitian with respect to a suitable inner product and hence plays the role of a Hamiltonian. Hence, because $\hat{H}_{cl} \cdot \mathbf{f} = i\frac{\partial \mathbf{f}}{\partial t}$ is formally equivalent to the Schrödinger equation, it is straightforward to extend the notion of Berry potential to *nondispersive* electromagnetic media [7,8].

As originally discussed by Raghu and Haldane [8], these ideas can be further generalized to dispersive loss-less media by introducing a generalized state vector $\mathbf{Q} = (\mathbf{Q}_0 \quad \mathbf{Q}_1 \quad \dots \quad \mathbf{Q}_\alpha \quad \dots)^T$ that describes the dynamics of the electromagnetic field and of the internal degrees of freedom of the material response (see also Refs. [32,33]). Here, $\mathbf{Q}_\alpha$ ($\alpha \geqslant 1$) represents the state variables associated with the internal degrees of freedom, and $\mathbf{Q}_0 = \mathbf{f}$. The result of Raghu and Haldane was derived under the assumption that the magneto-electric coupling tensors vanish ($\bar{\xi} = \bar{\zeta} = 0$) and that the material response is local [$\mathbf{M} = \mathbf{M}(\omega)$]. In Appendices A and B, it is shown that it is possible to further extend the findings of Ref. [8] to arbitrary lossless spatially dispersive materials. Specifically, Maxwell's equations (1) are shown to be equivalent to a generalized system of the form $\hat{L} \cdot \mathbf{Q} = i\frac{\partial}{\partial t}\mathbf{M}_g \cdot \mathbf{Q} + i\mathbf{j}_g$, with

$$\underbrace{\begin{pmatrix} \hat{N} + \sum_\alpha \text{sgn}(\omega_{p,\alpha})\mathbf{A}_\alpha^2 & |\omega_{p,1}|^{1/2}\mathbf{A}_1 & |\omega_{p,2}|^{1/2}\mathbf{A}_2 & \dots \\ |\omega_{p,1}|^{1/2}\mathbf{A}_1 & \omega_{p,1}\mathbf{1} & \mathbf{0} & \dots \\ |\omega_{p,2}|^{1/2}\mathbf{A}_2 & \mathbf{0} & \omega_{p,2}\mathbf{1} & \dots \\ \dots & \dots & \dots & \dots \end{pmatrix}}_{\hat{L}}$$
$$\cdot \underbrace{\begin{pmatrix} \mathbf{f} \\ \mathbf{Q}_1 \\ \mathbf{Q}_2 \\ \dots \end{pmatrix}}_{\mathbf{Q}} = i\frac{\partial}{\partial t}\underbrace{\begin{pmatrix} \mathbf{M}_\infty & \mathbf{0} & \mathbf{0} & \dots \\ \mathbf{0} & \mathbf{1} & \mathbf{0} & \dots \\ \mathbf{0} & \mathbf{0} & \mathbf{1} & \dots \\ \dots & \dots & \dots & \dots \end{pmatrix}}_{\mathbf{M}_g} \cdot \begin{pmatrix} \mathbf{f} \\ \mathbf{Q}_1 \\ \mathbf{Q}_2 \\ \dots \end{pmatrix} + i\underbrace{\begin{pmatrix} \mathbf{j} \\ \mathbf{0} \\ \mathbf{0} \\ \dots \end{pmatrix}}_{\mathbf{j}_g}, \tag{7}$$

where $\mathbf{1} \equiv \mathbf{1}_{6\times 6}$. As detailed in Appendix A, the 6×6 matrices $\mathbf{A}_\alpha$ are related to the residues of the material matrix $\mathbf{M}$ at the poles $\omega_{p,\alpha}$, and $\mathbf{M}_\infty = \lim_{\omega\to\infty}\mathbf{M}(\omega,\mathbf{k})$. Each pole of the system is associated with an auxiliary variable $\mathbf{Q}_\alpha$. In this paper, it is assumed that the high-frequency material response, $\mathbf{M}_\infty$, is independent of the wave vector and is positive definite. This assumption is rather natural because for high frequencies the response of realistic materials should reduce to that of the vacuum [26] (but we do not restrict ourselves to this case). Thus, $\mathbf{M}_g$ is also independent of the wave vector and is positive

definite. On the other hand, the operator $\hat{L}$ depends on the wave vector $\mathbf{k} = -i\nabla$, even for local media. Therefore, the dynamics of the generalized system is determined by

$$\hat{L}(-i\nabla) \cdot \mathbf{Q} = i\frac{\partial}{\partial t}\mathbf{M}_g \cdot \mathbf{Q} + i\mathbf{j}_g, \tag{8}$$

which is analogous to the Schrödinger equation in the absence of an external excitation ($\mathbf{j}_g = 0$). It is proven in Appendix B that for each fixed $\mathbf{k}$, the operator $\hat{H}_{cl} = \mathbf{M}_g^{-1} \cdot \hat{L}$ is Hermitian with respect to the weighted inner product

$$\langle \mathbf{Q}_B | \mathbf{Q}_A \rangle \equiv \tfrac{1}{2}\mathbf{Q}_B^* \cdot \mathbf{M}_g \cdot \mathbf{Q}_A. \tag{9}$$

Moreover, we show in Appendix B that if $\mathbf{Q}$ is a solution of the generalized system (8) with a space-time dependence of the type $e^{-i\omega t}e^{i\mathbf{k}\cdot\mathbf{r}}$, and if $\mathbf{f}$ denotes the corresponding solution of Maxwell's equations (1), then

$$\langle \mathbf{Q} | \mathbf{Q} \rangle \equiv \frac{1}{2}\mathbf{f}^* \cdot \frac{\partial}{\partial\omega}[\omega\mathbf{M}(\omega,\mathbf{k})] \cdot \mathbf{f}. \tag{10}$$

Hence, consistent with the discussion of Sec. II A, for fields with a space-time variation of the form $e^{-i\omega t}e^{i\mathbf{k}\cdot\mathbf{r}}$, the right-hand side of the above expression represents the stored energy density in the material and is always a positive quantity. In particular, $\langle \mathbf{Q} | \mathbf{Q} \rangle$ may be regarded as the (instantaneous) energy density of the dispersive material, and, importantly, for plane waves it can be written solely in terms of the electromagnetic fields $\mathbf{f} = (\mathbf{E} \quad \mathbf{H})^T$. This finding generalizes the results of Ref. [8].

C. The Berry potential

The generalized system (7) enables us to introduce a Berry potential $\mathcal{A}$ associated with a family of eigenmodes of a generic spatially dispersive material. To show this, we start by noting that the natural modes of (7) are the solutions of the eigenvalue problem

$$\hat{H}_{cl} \cdot \mathbf{Q} = \omega\mathbf{Q}, \tag{11}$$

with $\hat{H}_{cl} = \mathbf{M}_g^{-1} \cdot \hat{L}$, which, as previously discussed, is Hermitian with respect to the weighted inner product (9). The above equation is formally equivalent to the stationary Schrödinger equation with $\hbar = 1$. Therefore, the eigenmodes of $\hat{H}_{cl}$ span the whole Hilbert space wherein the state vector $\mathbf{Q}$ is defined, which has dimension $6 \times (N_p + 1)$, where N_p is the number of poles of $\mathbf{M}$. Moreover, any two eigenmodes associated with distinct eigenvalues are orthogonal with respect to the inner product in Eq. (9).

In this paper, we are interested in continuous media such that the material matrix $\mathbf{M}$ is independent of the spatial coordinates. As a consequence, the eigenmodes of Eq. (11) are of the form $\mathbf{Q}(\mathbf{r}) = \mathbf{Q}_\mathbf{k}e^{i\mathbf{k}\cdot\mathbf{r}}$ with the envelope $\mathbf{Q}_\mathbf{k}$ independent of $\mathbf{r}$. We denote the electromagnetic fields associated with $\mathbf{Q}(\mathbf{r})$ as $\mathbf{f}(\mathbf{r}) = \mathbf{f}_\mathbf{k}e^{i\mathbf{k}\cdot\mathbf{r}}$, where $\mathbf{f}_\mathbf{k}$ is the envelope of the electromagnetic fields, which for continuous media is also independent of $\mathbf{r}$. Importantly, Eq. (B2) determines a one-to-one mapping between the eigenmodes of Eq. (7) and the natural modes of Maxwell's equations (1), i.e., the solutions of

$$[\hat{N}(\mathbf{k}) - \omega\mathbf{M}(\omega,\mathbf{k})] \cdot \mathbf{f}_\mathbf{k} = 0, \tag{12}$$

where $\hat{N}(\mathbf{k})$ is defined as in Eq. (B1). Strictly speaking, the existence of this mapping is only guaranteed for waves with an eigenfrequency $\omega \neq \omega_{p,\alpha}$ because for $\omega = \omega_{p,\alpha}$ the mapping [Eq. (B2)] is singular. Modes of oscillation with $\omega = \omega_{p,\alpha}$ are dark modes in the sense that they are uncoupled from the electromagnetic field ($\mathbf{f} = 0$ but $\mathbf{Q} \neq 0$).

Let us now consider a smooth family of eigenmodes $\mathbf{Q}_{n\mathbf{k}}$ with the eigenfrequency $\omega_{n\mathbf{k}}$, such that the wave vector $\mathbf{k}$ lies in the $k_z = 0$ plane of wave vector space (i.e., the wave vector is of the form $\mathbf{k} = k_x \hat{\mathbf{x}} + k_y \hat{\mathbf{y}}$). Assuming the normalization $\langle \mathbf{Q}_{n\mathbf{k}} | \mathbf{Q}_{n\mathbf{k}} \rangle = 1$, the Berry potential $\mathcal{A}_{n\mathbf{k}}$ associated with this family of eigenmodes is defined as

$$\mathcal{A}_{n\mathbf{k}} = i \langle \mathbf{Q}_{n\mathbf{k}} | \partial_{\mathbf{k}} \mathbf{Q}_{n\mathbf{k}} \rangle, \tag{13}$$

where $\partial_{\mathbf{k}} = \frac{\partial}{\partial k_x} \hat{\mathbf{x}} + \frac{\partial}{\partial k_y} \hat{\mathbf{y}}$. It was demonstrated by Raghu and Haldane that the Berry potential can be written in terms of the electromagnetic field envelope $\mathbf{f}_{n\mathbf{k}}$ as in Refs. [7,8]

$$\mathcal{A}_{n\mathbf{k}} = \mathrm{Re}\left\{ i\, \mathbf{f}_{n\mathbf{k}}^* \cdot \frac{1}{2} \frac{\partial}{\partial \omega}(\omega \mathbf{M})_{\omega_{n\mathbf{k}}} \cdot \partial_{\mathbf{k}} \mathbf{f}_{n\mathbf{k}} \right\}. \tag{14}$$

In Appendix C, it is proven that this result also holds in the case of local media ($\mathbf{M} = \mathbf{M}(\omega)$) with a magneto-electric response characterized by nontrivial tensors $\bar{\bar{\xi}}, \bar{\bar{\zeta}}$. More generally, the formula applies to spatially dispersive media that satisfy some restrictions detailed in Appendix C, a particular case of which is the subclass of media with a response of the form

$$\mathbf{M}(\omega,\mathbf{k}) = \mathbf{M}_\infty + \frac{1}{1 + k^2/k_{\max}^2} \chi(\omega), \tag{15}$$

where $\mathbf{M}_\infty$ is a 6×6 (real-valued) tensor independent of frequency, $\chi(\omega)$ is a 6×6 susceptibility tensor dependent on frequency, $k^2 = \mathbf{k} \cdot \mathbf{k}$, and $k_{\max}$ is any real-valued constant and may be regarded as spatial cutoff frequency. In Sec. III, it will be discussed in detail why this particular form of the material response is interesting to us. For a general spatially dispersive material, one should use Eq. (C3) rather than Eq. (14), to calculate the Berry potential.

In summary, it was demonstrated that the theory of Refs. [7,8] can be generalized to spatially dispersive media and that the Berry potential of the subclass of media characterized by the material matrix (15) can be determined with Eq. (14), which only depends on the electromagnetic fields envelope $\mathbf{f}_{n\mathbf{k}}$.

III. CHERN NUMBERS IN CONTINUOUS MEDIA

The distinctive property of topological materials is that they are characterized by a topological invariant that depends on the band structure global properties. Specifically, it is possible to assign an integer (Chern) number to each subset of photonic bands separated by the remaining photonic bands by a complete bandgap [7–9,23],

$$\mathcal{C} = \frac{1}{2\pi} \iint dk_x dk_y \, \mathcal{F}_{\mathbf{k}}, \tag{16}$$

where $\mathcal{F}_{\mathbf{k}} = \frac{\partial \mathcal{A}_x}{\partial k_y} - \frac{\partial \mathcal{A}_y}{\partial k_x}$ is the Berry curvature. Crucially, the Chern number is absolutely insensitive to weak perturbations of the material microstructure, e.g., to weak perturbations of the shape of the structural unities forming a photonic crystal.
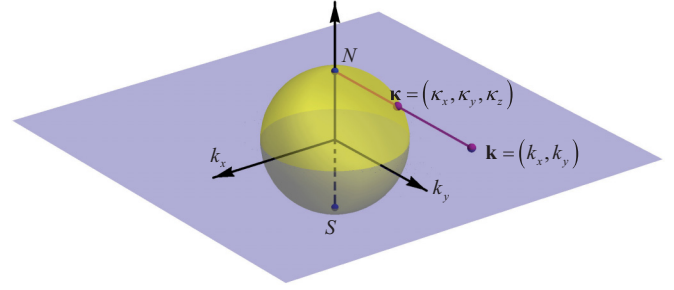

FIG. 1. (Color online) The stereographic projection and the Riemann sphere. The (k_x, k_y) plane plus the point $\mathbf{k} = \infty$ can be mapped into a spherical surface with unit radius. The point $\mathbf{k} = \infty$ is mapped into the north pole of the sphere.

The only way to change the topological invariant is to close the band gap. Because of this property, when two topologically distinct photonic crystals that share a complete bandgap are put together, topologically protected unidirectional edge states at the interface of these crystals may appear [7,9].

The most common topological classification of solid-state materials relies on the quite restrictive assumption that the relevant structure is periodic [9]. The reason is mainly technical: to guarantee that the topological invariant is an integer, the relevant wave vector space must be a closed surface with no boundary. For example, in a photonic crystal, the wave vector space is the Brillouin zone [2], which is isomorphous to a torus (a closed surface with no boundary). In contrast, in a continuous material, the wave vector is defined over an unbounded open region, $k_x, k_y \in (-\infty, +\infty)$; hence, in general, it is not possible to calculate Chern invariants in continuous media. In the following, it is proven that it is possible to overcome these difficulties and to define topological invariants for dispersive continuous media.

A. The Riemann sphere

A useful idea is to map the (k_x, k_y) plane into the Riemann sphere (Fig. 1), which is evidently a closed surface. Specifically, each point $\mathbf{k} = (k_x, k_y, 0)$ can be mapped into a point $\boldsymbol{\kappa} = (\kappa_x, \kappa_y, \kappa_z)$ of the unit radius sphere surface by the *stereographic projection* as

$$(k_x, k_y) \rightarrow \boldsymbol{\kappa} = \frac{1}{k^2 + 1}(2k_x, 2k_y, k^2 - 1), \tag{17}$$

where $k^2 = \mathbf{k} \cdot \mathbf{k} = k_x^2 + k_y^2$.

As illustrated in Fig. 1, the point $\boldsymbol{\kappa} = (\kappa_x, \kappa_y, \kappa_z)$ is the intersection of the spherical surface with a line passing through both the sphere's north pole ($N = (0,0,1)$) and the point $\mathbf{k}$. For example, the origin of the $\mathbf{k}$ space is mapped into the sphere's south pole ($S = (0,0,-1)$). In this discussion, it is implicit that the plane of propagation is the xoy plane. This choice may be different, and in general it is possible to calculate Chern numbers for any plane in the $\mathbf{k}$ space passing through the origin.

Crucially, the stereographic projection determines a one-to-one mapping of the unit radius spherical surface *excluding* the north pole into the (k_x, k_y) plane (with k_x, k_y finite). The problem that remains is that the spherical surface minus one

point (the north pole) is *not* a compact surface without boundary. This can, however, be partially remedied by mapping the north pole into the infinity ($\mathbf{k} = \infty$). Hence, as is well known, the (k_x, k_y) plane together with the point $\mathbf{k} = \infty$ are isomorphous to the Riemann sphere.

This discussion shows that the pseudo-Hamiltonian of the system, $\hat{H}_{cl,\mathbf{k}}$, may be regarded as being defined over the Riemann sphere (unit radius spherical surface of the κ space), which is a compact surface with no boundary. Thus, provided that the $\hat{H}_{cl,\mathbf{k}}$ is *sufficiently well-behaved* in the vicinity of the north pole ($\mathbf{k} = \infty$)—and usually it is not—the Chern number associated with any subset of photonic bands is an integer.

B. An example

Before elucidating about the conditions under which the Hamiltonian may be well behaved at the north pole, let us consider a specific example to illustrate the discussion and the difficulties. Specifically, we consider a nonreciprocal continuous medium characterized by the permittivity and permeability tensors,

$$\bar{\varepsilon} = \begin{pmatrix} \varepsilon_{11} & \varepsilon_{12} & 0 \\ \varepsilon_{21} & \varepsilon_{22} & 0 \\ 0 & 0 & \varepsilon_{33} \end{pmatrix}, \quad \bar{\mu} = \mathbf{1}, \quad (18a)$$

$$\varepsilon_{11} = \varepsilon_{22} = 1 + \frac{\omega_0 \omega_e}{\omega_0^2 - \omega^2},$$

$$\varepsilon_{12} = -\varepsilon_{21} = \frac{-i\omega_e \omega}{\omega_0^2 - \omega^2}, \quad \varepsilon_{33} = 1, \quad (18b)$$

and by a trivial magnetoelectric coupling $\bar{\xi} = \bar{\zeta} = 0$. In the above, $|\omega_0|$ is the resonance frequency, and ω_e determines the resonance strength. Provided that these parameters satisfy $\omega_0 \omega_e > 0$, the corresponding material matrix $\mathbf{M}$ [Eq. (3)] satisfies the conditions in Eqs. (4)–(6). The parameter ω_0 may be either positive or negative. Note that the material parameters are independent of the wave vector, and hence the material response is local. This type of material response is similar to that that characterizes conventional bulk magnetized materials at optics (e.g., bismuth iron garnet [34]), and the sign of ω_e depends on the orientation of the bias magnetic field. Crucially, the permittivity tensor [Eq. (18)] is not symmetric, and thus it models a nonreciprocal material. It is well known that for lossless systems, a nonreciprocal response is equivalent to a broken time reversal symmetry. Note that the Chern numbers of a system with the time-reversal symmetry (e.g., standard reciprocal dielectrics and metals) vanish because $\mathcal{F}_{\mathbf{k}} = -\mathcal{F}_{-\mathbf{k}}$ [8,9].

For propagation in the *xoy* plane, $\mathbf{k} = (k_x, k_y, 0)$, the plane waves supported by the medium [Eq. (11)] decouple into transverse electric (TE) waves (with $E_z \neq 0$ and $H_z = 0$) and transverse magnetic (TM) waves (with $E_z = 0$ and $H_z \neq 0$). The dispersion of the corresponding photonic modes is given by

$$k^2 = \frac{\varepsilon_{11}^2 + \varepsilon_{12}^2}{\varepsilon_{11}} \left(\frac{\omega}{c}\right)^2, \quad \text{(TM modes)}, \quad (19a)$$

$$k^2 = \varepsilon_{33} \left(\frac{\omega}{c}\right)^2, \quad \text{(TE modes)}. \quad (19b)$$

The associated electromagnetic modes have envelopes $(\mathbf{f}(\mathbf{r}) = \binom{\mathbf{E}}{\mathbf{H}} = \mathbf{f}_{\mathbf{k}} e^{i\mathbf{k}\cdot\mathbf{r}})$ such that

$$\mathbf{f}_{n\mathbf{k}} = \begin{pmatrix} \bar{\varepsilon}^{-1} \cdot \left(\hat{\mathbf{z}} \times \frac{\mathbf{k}}{\varepsilon_0 \omega_{n\mathbf{k}}}\right) \\ \hat{\mathbf{z}} \end{pmatrix}, \quad \text{(TM modes)}, \quad (20a)$$

$$\mathbf{f}_{n\mathbf{k}} = \begin{pmatrix} \hat{\mathbf{z}} \\ \frac{\mathbf{k}}{\mu_0 \omega_{n\mathbf{k}}} \times \hat{\mathbf{z}} \end{pmatrix}, \quad \text{(TE modes)}. \quad (20b)$$

These field envelopes are not normalized. In the above, $\omega_{n\mathbf{k}}$ represent the solutions of the pertinent dispersion equation [Eq. (19)]. Because the material matrix $\mathbf{M}$ has $N_p = 2$ poles (at $\omega = \pm\omega_0$), there are a total of $6 \times (N_p + 1) = 18$ branches of solutions of the eigensystem (11). The index n in Eq. (20) identifies a specific branch. Because of the reality condition (6), each branch of positive frequency natural modes ($\omega_{n\mathbf{k}} > 0$) can be paired with a branch of negative frequency ($\omega_{n\mathbf{k}} < 0$) eigenvalues. It may be checked that Eq. (19a) [Eq. (19b)] is associated with two (one) branches of positive frequency eigenvalues, respectively. Moreover, there are two static-type branches of longitudinal modes with $\omega_{n\mathbf{k}} = 0$. Hence, Eqs. (19a) and (19b) predict a total of eight branches of eigenmodes, including the positive-, negative-, and zero-frequency eigenmodes. The missing $18 - 8 = 10$ branches of solutions of the eigensystem (11) are necessarily dark modes associated with the two poles $\omega_{n\mathbf{k}} = \pm\omega_0$ and have a trivial electromagnetic field. Indeed, as discussed below Eq. (12), generally there is a one-to-one mapping between the natural modes of the eigensystems (11) and (12), with the possible exception of solutions with $\omega = \omega_{p,\alpha}$. These branches do not contribute to the Berry potential (because the corresponding eigenmodes $\mathbf{Q_k}$ are independent of $\mathbf{k}$) and hence are ignored from hereafter.

Figure 2(a) depicts the band diagram of the TM- and TE-polarized eigenwaves with positive frequencies for the case $\omega_e = 0.5\omega_0$. The dispersion of the TE natural modes (dashed line) follows the light line. Differently, the TM eigenwaves are organized into two branches separated by a band gap.

We calculated the Chern number associated with each of the positive frequency branches. As discussed in Appendix D, the Chern number in the Riemann sphere can be simply computed with the standard formula (16) (being the integration region the entire (k_x, k_y) plane), which is written in terms of the standard Berry potential $\mathcal{A}_{\mathbf{k}}$ in the plane. This is analogous to what happens in the periodic case [7], wherein notwithstanding the wave vector space is effectively a torus all the calculations are usually done using the Berry potential defined over the (k_x, k_y) plane. Because the envelopes of the electromagnetic field in Eq. (20) are not normalized, the Berry potential is computed using [compare with Eq. (14)]

$$\mathcal{A}_{n\mathbf{k}} = \frac{\text{Re}\left\{i\, \mathbf{f}_{n\mathbf{k}}^* \cdot \frac{\partial}{\partial\omega}[\omega\mathbf{M}(\omega,\mathbf{k})]_{\omega_{n\mathbf{k}}} \cdot \partial_{\mathbf{k}} \mathbf{f}_{n\mathbf{k}}\right\}}{\mathbf{f}_{n\mathbf{k}}^* \cdot \frac{\partial}{\partial\omega}[\omega\mathbf{M}(\omega,\mathbf{k})]_{\omega_{n\mathbf{k}}} \cdot \mathbf{f}_{n\mathbf{k}}}. \quad (21)$$

For completeness, the relation between the Berry potential calculated in the plane and the Berry potential defined over the Riemann sphere is given in Appendix D.

One important point is that the basis of wave functions determined by Eq. (20) is globally defined, except at the points $k = 0$ and $k = \infty$. Consequently, the Berry potential
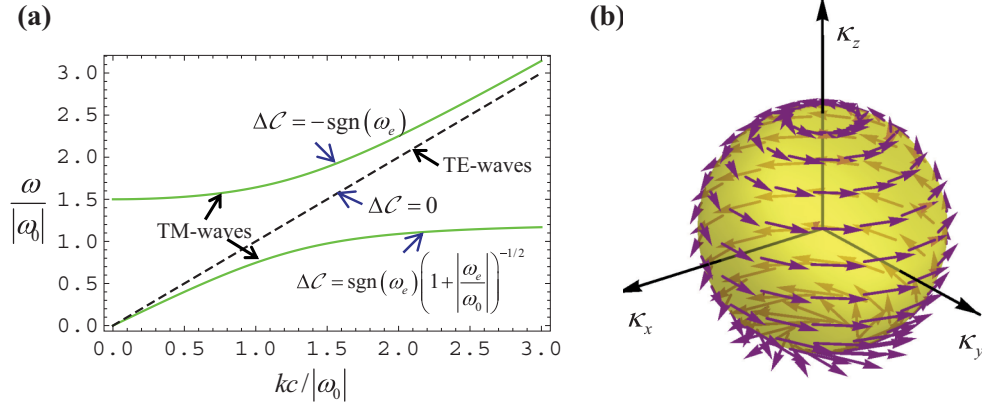
FIG. 2. (Color online) Band diagram and Berry potential for a magneto-optic material. (a) Band diagram ω vs k for a material characterized by the material parameters (18) with $\omega_e = 0.5\omega_0$. (b) Representation in the Riemann sphere of the Berry potential associated with the high-frequency TM branch for the particular basis of wave functions defined by Eq. (20).

$\mathcal{A}_\mathbf{k}$ associated with this specific basis is also globally defined, except at the origin and infinity (in the Riemann sphere the Berry potential is globally defined except at the north and south poles). Hence, from Stoke's theorem, it is possible to write the Chern number associated with nth eigenmode branch as

$$\Delta\mathcal{C}_n = \frac{1}{2\pi}\oint_{k=\infty}\mathcal{A}_{n\mathbf{k}}\cdot\mathbf{dl} - \frac{1}{2\pi}\oint_{k=0^+}\mathcal{A}_{n\mathbf{k}}\cdot\mathbf{dl}, \quad (22)$$

where the two line integrals are over circles of infinite and infinitesimal radii, respectively. Because our system is invariant under arbitrary rotations about the z axis, $\mathcal{A}_{n\mathbf{k}}\cdot\mathbf{dl} = \mathcal{A}_{n,\varphi}k\,d\varphi$ is independent of φ. Here, (k,φ) defines a system of polar coordinates in the $\mathbf{k}$ plane, and $\mathcal{A}_{n,\varphi} = \mathcal{A}_{n\mathbf{k}}\cdot\hat{\varphi}$. Hence, it follows that

$$\Delta\mathcal{C}_n = \lim_{k\to\infty}(\mathcal{A}_{n,\varphi=0}k) - \lim_{k\to 0^+}(\mathcal{A}_{n,\varphi=0}k). \quad (23)$$

Using this formalism, it is straightforward to prove (the computational details are omitted for conciseness) that $\Delta\mathcal{C}_n = 0$ for the TE-waves branch, that $\Delta\mathcal{C}_n = -\text{sgn}(\omega_e)$ for the high-frequency TM-waves branch, and that $\Delta\mathcal{C}_n = +\text{sgn}(\omega_e)(1 + |\frac{\omega_e}{\omega_0}|)^{-1/2}$ for the low-frequency TM-waves branch. Here, $\text{sgn} = \pm$ stands for the sign of a real number.

This simple example shows that in general the Chern numbers associated with continuous media are *not* integers. Particularly, the Chern number associated with the low-frequency TM branch is never an integer for $\omega_e \neq 0$. It will be seen in the next subsections that the problem is that the pseudo-Hamiltonian of the medium is not sufficiently well behaved at infinity, and we will explain how this can be fixed in a simple manner.

Crucially, the Chern number associated with the high-frequency TM-waves branch is always an integer, $\Delta\mathcal{C}_n = \pm 1$. Figure 2(b) shows a representation of the corresponding Berry potential in the Riemann sphere. The Berry potential is calculated with Eq. (D2) using the basis of eigenmodes [Eq. (20)]. As seen, the Berry potential is an azimuthal field with rotational symmetry about the vertical axis. It is important to underline that the Berry potential (unlike the Berry curvature) is not Gauge invariant [23], and hence the representation of Fig. 2(b) is only valid for the very particular basis (20). This particular Berry potential vanishes at the north

pole ($k = \infty$) because the material response is asymptotically the same as the vacuum, i.e., $\bar{\varepsilon} \to \mathbf{1}$ as $\omega \to \infty$. On the other hand, the Berry potential has a singularity at the south pole ($k = 0$), which determines the nonzero Chern number.

C. A condition for the existence of integer Chern numbers

Let us consider now an arbitrary closed contour C in the (k_x, k_y) plane and two arbitrary bases of eigenmodes ($\mathbf{f}_{n\mathbf{k}}$) and ($\mathbf{f}'_{n\mathbf{k}}$) that vary smoothly with the wave vector in the vicinity of the contour C. Let $\mathcal{A}_\mathbf{k}$ and $\mathcal{A}'_\mathbf{k}$ be the Berry potentials associated with each eigenmode basis. Since the two bases must differ by a Gauge transformation, $\mathbf{f}'_{n\mathbf{k}} = \mathbf{f}_{n\mathbf{k}}e^{i\theta_{n\mathbf{k}}}$, it follows that $\mathcal{A}'_\mathbf{k} = \mathcal{A}_\mathbf{k} - \partial_\mathbf{k}\sum_n\theta_{n\mathbf{k}}$ and hence, as it is well-known, the difference of the Berry phases must be an integer multiple of 2π [23]:

$$\oint_C (\mathcal{A}_\mathbf{k} - \mathcal{A}'_\mathbf{k})\cdot\mathbf{dl} = 2\pi m, \quad m \text{ is an integer.} \quad (24)$$

Consider next the particular case wherein C_R is a circle with an arbitrarily small radius $R = 0^+$ centered on some point of interest $\mathbf{k}_0$. Provided the Hamiltonian of the system varies smoothly in the vicinity of $\mathbf{k}_0$, as is usually the case, there is a basis of eigenfunctions ($\mathbf{f}'_{n\mathbf{k}}$) that is smooth in a neighborhood of $\mathbf{k}_0$ (including at $\mathbf{k}_0$). Hence, the corresponding Berry potential $\mathcal{A}'_\mathbf{k}$ is also free of singularities and is smooth in the vicinity of the circle C_R and in its interior. Since by hypothesis $C_{R=0^+}$ is a circle with arbitrarily small radius, it follows that the corresponding Berry phase vanishes, $\oint_{C_{R=0^+}}\mathcal{A}'_\mathbf{k}\cdot\mathbf{dl} = 0$. Thus, for an arbitrary basis of wave functions ($\mathbf{f}_{n\mathbf{k}}$) defined in the vicinity of $\mathbf{k}_0$, one has

$$\oint_{C_{R=0^+}}\mathcal{A}_\mathbf{k}\cdot\mathbf{dl} = 2\pi m, \quad m \text{ is an integer.} \quad (25)$$

Note that a general ($\mathbf{f}_{n\mathbf{k}}$) may not be smooth at $\mathbf{k}_0$ (it may be singular at $\mathbf{k}_0$) and is only required to be smooth in a vicinity of $C_{R=0^+}$.

Even though the previous discussion was focused on the $\mathbf{k}$ plane, it can be readily generalized to the Riemann sphere. In that case, there is a point of particular interest: the north pole. A circle with infinitesimal radius centered on the north pole is

mapped into a circle of infinite radius in the plane. Thus, if the Hamiltonian varies smoothly at the north pole of the sphere, it follows that for an arbitrary Berry potential defined in the vicinity of $k = \infty$,

$$\oint_{k=\infty} \mathcal{A}_{\mathbf{k}} \cdot \mathbf{dl} = 2\pi m, \quad m \text{ is an integer.} \qquad (26)$$

In the above, the line integral is taken over a circle with infinite radius in the plane.

Motivated by these ideas, we say that a Hamiltonian is well-behaved at the north pole of the sphere when there is a basis of eigenfunctions $(\mathbf{f}_{n\mathbf{k}})$ defined in the vicinity of the north pole (i.e., in the vicinity of $k = \infty$) for which the corresponding Berry potential satisfies Eq. (26). Note that from the previous discussion, if Eq. (26) is satisfied by a given basis of eigenfunctions then it will also be satisfied by any other basis $(\mathbf{f}'_{n\mathbf{k}})$ that differs from $(\mathbf{f}_{n\mathbf{k}})$ by a smooth Gauge transformation (the integer m, however, depends on the Gauge). Also note that the well-behaved condition is less demanding than imposing that the Hamiltonian is smooth at the north pole.

Generally, if the Hamiltonian is smooth everywhere in the Riemann sphere (with the possible exception of the north pole) and is well behaved at the north pole (in the sense explained above), then the Chern number is an integer. Indeed, similar to the example considered in the previous subsection, typically there is a basis of eigenfunctions $(\mathbf{f}_{n\mathbf{k}})$ globally smooth everywhere except at a few singular (Gauge-dependent) points on the Riemann sphere (one of them is typically the north pole). Thus, using the Stoke's theorem, the Chern number can be written as summation of line integrals, $\mathcal{C} = \frac{1}{2\pi}(-\sum_{\mathbf{k}_i} \oint_{C_{R=0^+}(\mathbf{k}_i)} \mathcal{A}_{\mathbf{k}} \cdot \mathbf{dl} + \oint_{k=\infty} \mathcal{A}_{\mathbf{k}} \cdot \mathbf{dl})$. The first addend gives the contribution of the singular points $\mathbf{k}_i$ in the finite (k_x, k_y) plane, and the second addend gives the contribution of the north pole ($k = \infty$). Because by hypothesis the Hamiltonian is smooth for any finite $\mathbf{k}_i$, the first addend is a multiple of 2π. On the other hand, if the Hamiltonian is well behaved at infinity, the second addend has the same property because of Eq. (26). Thus, $\mathcal{C}$ is really an integer, as we wanted to prove.

The above ideas readily explain why in the example of the previous subsection the high-frequency TM branch gives an integer contribution to the Chern number [$\Delta\mathcal{C}_n = -\mathrm{sgn}(\omega_e) = \pm 1$]. The reason is that the high-frequency branch is such that $\omega \to \infty$ as $k \to \infty$, and as a consequence the material response for this eigenmode branch approaches that of the vacuum ($\bar{\varepsilon} \to \mathbf{1}$) in the vicinity of the north pole. This indicates that it is possible to choose a basis of eigenfunctions $(\mathbf{f}_{n\mathbf{k}})$ such that $(\mathbf{f}_{n\mathbf{k}}) \approx (\mathbf{f}_{n\mathbf{k}}^{\mathrm{vac}})$ in the limit $k \to \infty$, where $(\mathbf{f}_{n\mathbf{k}}^{\mathrm{vac}})$ is some arbitrary basis of eigenfunctions associated with the vacuum ($\bar{\varepsilon} = \mathbf{1}, \bar{\mu} = \mathbf{1}$). Thus, for $k \to \infty$, the Berry potential should satisfy $\mathcal{A}_{\mathbf{k}} = \mathcal{A}_{\mathbf{k}}^{\mathrm{vac}}$, where $\mathcal{A}_{\mathbf{k}}^{\mathrm{vac}}$ is the Berry potential associated with $(\mathbf{f}_{n\mathbf{k}}^{\mathrm{vac}})$. Importantly, in the vacuum case it is possible to choose $(\mathbf{f}_{n\mathbf{k}}^{\mathrm{vac}})$ real valued so that $\mathcal{A}_{\mathbf{k}}^{\mathrm{vac}}$ vanishes. Therefore, the preceding arguments show that for high-frequency branches (with $\omega_{n\mathbf{k}} \to \infty$), the eigenfunctions $(\mathbf{f}_{n\mathbf{k}})$ can be identified with those of the vacuum when $k \to \infty$ and hence may be chosen such that the integral in Eq. (26) vanishes. As a consequence, these bands have an integer Chern number, consistent with the previous subsection.

D. A wave vector cutoff for the material response

The results of Sec. III B show that a Berry potential associated with the low-frequency eigenmode branches of a dispersive continuous material typically does not satisfy Eq. (26). Thus, in general the corresponding Chern number is not an integer. Next, we show that it is possible to modify the material response in a physically intuitive and justifiable manner to fix this problem.

Our solution is motivated by the finding that the high-frequency eigenmode branches give an integer contribution to the Chern number. This can be attributed to the fact that for these branches the material matrix approaches $\mathbf{M} \to \mathbf{M}_\infty$ as $k \to \infty$ (in the vicinity of the north pole), where $\mathbf{M}_\infty = \lim_{\omega \to \infty} \mathbf{M}(\omega)$ determines the high-frequency response of the medium. As shown in the previous subsection, this property guarantees the existence of a Berry potential for which Eq. (26) is satisfied for the high-frequency branches and thus ensures an integer Chern number. More generally, the same conclusion remains valid if $\mathbf{M}_\infty$ coincides with the material matrix of any anisotropic dispersionless material. Indeed, analogous to the vacuum case, because $\mathbf{M}_\infty$ is necessarily real valued, it is possible to pick a Gauge for which the Berry potential vanishes.

Crucially, the situation is quite different for the low-frequency eigenmode branches. Indeed, for these branches $\omega_{n\mathbf{k}}$ has the asymptotic form $\omega_{n\mathbf{k}} \to \omega_{n,\infty} = const.$ as $k \to \infty$, and hence $\mathbf{M} \to \mathbf{M}(\omega_{n,\infty})$, which may be very different from the material matrix of the vacuum and usually is complex valued. In other words, within a local formalism the material response is independent of the wave vector, and hence it persists even for arbitrarily fast spatial variations of the electromagnetic fields ($k \to \infty$). From a physical point of view, such a situation is not likely to happen. In a realistic material, a field with a very fast spatial variation cannot effectively polarize the microscopic constituents of the medium, and hence the material response is expected to vanish when $k \to \infty$.

The emergence of a wave vector cutoff is well understood in some materials. For example, a lossless electron gas described by a drift-diffusion model has a spatially dispersive response such that the permittivity seen by the transverse waves is $\varepsilon_T/\varepsilon_0 = 1 - \omega_p^2/\omega^2$, whereas the permittivity seen by the longitudinal waves is $\varepsilon_L/\varepsilon_0 = 1 - \omega_p^2/(\omega^2 - v^2 k^2)$, where ω_p is the plasma frequency and v is a parameter with unities of velocity that depends on the diffusion coefficient [35,36]. Hence, in the limit $k \to \infty$ the longitudinal permittivity approaches the response of the vacuum $\varepsilon_L/\varepsilon_0 \to 1$, i.e., the response to longitudinal waves has a wave vector cutoff. In this specific physical system, the wave vector cut-off for longitudinal oscillations is a consequence of the diffusion effects which act to avoid the localization of the electrons over distances smaller than some characteristic diffusion length.

Inspired by this result, we may introduce a high-frequency spatial cutoff by transforming a local material response [described by the matrix $\mathbf{M}(\omega)$] as

$$\mathbf{M}_{\mathrm{reg}}(\omega, \mathbf{k}) = \mathbf{M}_\infty + \frac{1}{1 + k^2/k_{\mathrm{max}}^2}[\mathbf{M}(\omega) - \mathbf{M}_\infty], \qquad (27)$$

where $\mathbf{M}_\infty = \lim_{\omega \to \infty} \mathbf{M}(\omega)$. Such a regularized material response is consistent with Eq. (15), being $\chi(\omega) = \mathbf{M}(\omega) - \mathbf{M}_\infty$

the local material susceptibility matrix. The wave vector cutoff is determined by the parameter $k_{\max}$, which can be arbitrarily large. Clearly, for $k \ll k_{\max}$, the transformed material matrix is nearly coincident with the original material matrix: $\mathbf{M}_{\mathrm{reg}}(\omega,\mathbf{k}) \approx \mathbf{M}(\omega)$. The local and the nonlocal responses differ only for large values of k (comparable to $k_{\max}$). Importantly, within the proposed nonlocal framework, the material response ceases in the $k \to \infty$ limit ($\lim_{k \to \infty} \mathbf{M}_{\mathrm{reg}}(\omega,\mathbf{k}) = \mathbf{M}_{\infty}$), similar to what happens in the $\omega \to \infty$ limit. This suggests that for a material response of the form (15), the Hamiltonian is

well behaved at the north pole and that the Chern number of any subset of eigenmode branches is an integer.

To demonstrate this property, first we note that $\mathbf{M}_{\mathrm{reg}}$ and $\mathbf{M}$ have precisely the same poles, $\omega_{p,\alpha}$, whereas the residues differ simply by a scaling factor $1/(1 + k^2/k_{\max}^2)$. Hence, from Appendix A it is seen that $\mathbf{A}_{\alpha}$ is transformed as $\mathbf{A}_{\alpha} \to \mathbf{A}_{\alpha}/(1 + k^2/k_{\max}^2)^{1/2}$. Thus, the pseudo-Hamiltonian associated with the regularized material response $\mathbf{M}_{\mathrm{reg}}$ is of the form $\hat{H}_{cl,\mathrm{reg}} = \mathbf{M}_g^{-1} \cdot \hat{L}_{\mathrm{reg}}$, with $\mathbf{M}_g$ defined as in Eq. (7) and $\hat{L}_{\mathrm{reg}}$ given by [compare with $\hat{L}$ in Eq. (7)]

$$\hat{L}_{\mathrm{reg}} = \begin{pmatrix} \hat{N} + \frac{1}{1+k^2/k_{\max}^2}\sum_{\alpha}\mathrm{sgn}(\omega_{p,\alpha})\mathbf{A}_{\alpha}^2 & \frac{1}{(1+k^2/k_{\max}^2)^{1/2}}|\omega_{p,1}|^{1/2}\mathbf{A}_1 & \frac{1}{(1+k^2/k_{\max}^2)^{1/2}}|\omega_{p,2}|^{1/2}\mathbf{A}_2 & ... \\ \frac{1}{(1+k^2/k_{\max}^2)^{1/2}}|\omega_{p,1}|^{1/2}\mathbf{A}_1 & \omega_{p,1}\mathbf{1} & \mathbf{0} & ... \\ \frac{1}{(1+k^2/k_{\max}^2)^{1/2}}|\omega_{p,2}|^{1/2}\mathbf{A}_2 & \mathbf{0} & \omega_{p,2}\mathbf{1} & ... \\ ... & ... & ... & ... \end{pmatrix}. \tag{28}$$

For a local material, $\mathbf{A}_{\alpha}$ and $\omega_{p,\alpha}$ are independent of the wave vector. Hence, the asymptotic form of $\hat{L}_{\mathrm{reg}}$ is simply

$$\hat{L}_{\mathrm{reg}} \underset{k \to \infty}{\approx} \begin{pmatrix} \hat{N} & \mathbf{0} & \mathbf{0} & ... \\ \mathbf{0} & \omega_{p,1}\mathbf{1} & \mathbf{0} & ... \\ \mathbf{0} & \mathbf{0} & \omega_{p,2}\mathbf{1} & ... \\ ... & ... & ... & ... \end{pmatrix}. \tag{29}$$

This shows that the eigenvalues of $\hat{H}_{cl,\mathrm{reg}}$ for large k are either those of the vacuum ($\omega_{\mathbf{k}} \approx ck$, determined by the operator $\hat{N}$) or coincident with the poles of the material response, $\omega_{\mathbf{k}} \approx \omega_{p,\alpha}$. In either case, the corresponding eigenvectors may always be chosen real valued. Thus, it is possible to pick a Gauge such that the eigenmodes $\mathbf{Q}_{n\mathbf{k}}$ are real valued in the limit $k \to \infty$. Evidently, the corresponding Berry potential [Eq. (13)] vanishes at the north pole and thus satisfies the condition (26) with $m = 0$. Thus, it follows that $\hat{H}_{cl,\mathrm{reg}}$ is well behaved at the north pole, as we wanted to show.

These ideas can be readily generalized to a wide class of spatially dispersive media described by a material matrix $\mathbf{M} = \mathbf{M}(\omega,\mathbf{k})$. If the Hamiltonian $\hat{H}_{cl,\mathbf{k}} = \mathbf{M}_g^{-1} \cdot \hat{L}_{\mathbf{k}}$ [with $\hat{L} = \hat{L}_{\mathbf{k}}$ defined as in Eq. (7)] is a smooth function in the (k_x, k_y) plane, and if $\mathbf{A}_{\alpha,\mathbf{k}}$ and $\omega_{p,\alpha,\mathbf{k}}$ in Eq. (7) satisfy $\lim_{k \to \infty}|\omega_{p,\alpha,\mathbf{k}}|^{1/2}\mathbf{A}_{\alpha,\mathbf{k}} = 0$ and $\lim_{k \to \infty}\mathbf{A}_{\alpha,\mathbf{k}}^2 = 0$, then the Chern numbers associated with $\mathbf{M} = \mathbf{M}(\omega,\mathbf{k})$ are integers. In general, these restrictions can be enforced by introducing a suitable spatial cutoff, analogous to Eq. (27). The cutoff factor is generally of the form $(1 + k^2/k_{\max}^2)^{-m}$, where $m \geqslant 1$ depends on the asymptotic behavior of $\mathbf{M}(\omega,\mathbf{k})$ for large k.

IV. DISCUSSION AND EXAMPLES

The theory developed in the previous section demonstrates that if we restrict ourselves to the subclass of pseudo-Hamiltonians $\hat{H}_{cl,\mathbf{k}}$ smooth in the (k_x, k_y) plane and well-behaved at infinity (at the north pole), then it is possible to calculate Chern numbers. It was seen that while in general a material response of the form $\mathbf{M} = \mathbf{M}(\omega)$ is not associated with a Hamiltonian with the required properties, it is possible to regularize it by introducing a high spatial-frequency cutoff.

At this stage it is important to highlight that when $\mathbf{M}(\omega)$ is a real-valued matrix for ω real valued, then $\hat{H}_{cl,\mathbf{k}}$ is already well behaved at infinity, even without the spatial cutoff. The reason is that in such circumstances, the operator $\hat{L}$ is real valued; hence, in general it is possible to pick a Gauge of real-valued eigenfunctions for which the Berry potential identically vanishes at infinity. Hence, local material responses with $\mathbf{M}(\omega)$ real valued are associated with well-behaved Hamiltonians. For example, an isotropic dispersive lossless dielectric with permittivity $\varepsilon(\omega)$ and permeability $\mu(\omega)$ determines always a well-behaved Hamiltonian and hence belongs to the subclass of interest.

An important property is that if $\mathbf{M}_1(\omega,\mathbf{k})$ and $\mathbf{M}_2(\omega,\mathbf{k})$ are arbitrary material responses associated with well-behaved Hamiltonians, then the combined material response, $\tilde{\mathbf{M}}(\omega,\mathbf{k}) = \mathbf{M}_{\infty} + c_1\chi_1(\omega,\mathbf{k}) + c_2\chi_2(\omega,\mathbf{k})$, with $c_1, c_2 \geqslant 0$ also is. Here, $\chi_i(\omega,\mathbf{k}) = \mathbf{M}_i(\omega,\mathbf{k}) - \mathbf{M}_{\infty}$ ($I = 1,2$) are susceptibilities associated with the relevant materials, which are assumed to satisfy $\lim_{k \to \infty}\chi_i(\omega,\mathbf{k}) = \chi_{i,\infty}(\omega)$ being $\chi_{i,\infty}(\omega)$ some real-valued matrix for ω real valued. The constants c_1, c_2 need to be nonnegative so that $\tilde{\mathbf{M}}$ satisfies the condition (5). The enunciated property is a consequence of the fact that the elements of $\hat{L}$ [Eq. (7)] only depend on the poles and on the residues of $\tilde{\mathbf{M}}$ (which are evidently the mix of the poles and residues of the individual material responses) and of the fact that asymptotically (as $k \to \infty$) $\hat{L}$ is real valued because $\lim_{k \to \infty}\chi_i(\omega,\mathbf{k}) = \chi_{i,\infty}(\omega)$.

The above discussion demonstrates that the subspace of well-behaved Hamiltonians is quite rich and that any two well-behaved Hamiltonians can be continuously deformed one into the other without leaving the subclass of interest. In the following subsections, we illustrate the application of the developed theory and explain how it can be used to predict the propagation of edge states.

A. Magneto-optic material

Armed with this theory, we return to the example of Sec. III B. Figure 3 depicts the band diagram of the same magneto-optic material for different values of the cutoff frequency $k_{\max}$. We only show the positive-frequency bands
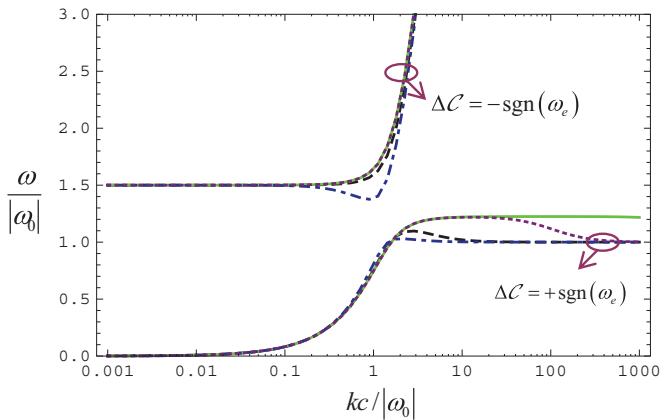
FIG. 3. (Color online) Effect of the high-frequency spatial cutoff on the band structure. Band diagram ω vs k (TM waves) for a magneto-optic material characterized by the material parameters (18) with $\omega_e = 0.5\omega_0$ and (i) (green solid lines) no spatial cutoff, (ii) (purple dotted lines) $k_{\max} = 100|\omega_0|/c$, (iii) (black dashed lines) $k_{\max} = 3|\omega_0|/c$, and (iv) (blue dot-dashed lines) $k_{\max} = |\omega_0|/c$.

associated with TM-waves (the band associated with TE waves is unaffected by the cutoff).

As seen in Fig. 3, for $k \ll k_{\max}$ the band structure calculated with the cutoff (purple, black, and blue lines) is nearly coincident with the band structure of the original magneto-optic material (green lines, for which $k_{\max} = \infty$). The coincidence can be made as good as one wishes by increasing $k_{\max}$. Importantly, the high-frequency band structure is significantly affected by the spatial cutoff. Particularly, it can be checked that in this example the dispersion of the first branch ω_k approaches $\lim_{k \to \infty} \omega_k = |\omega_0|$ when a cutoff is imposed ($k_{\max}$ finite), while without the cutoff ($k_{\max} = \infty$) $\lim_{k \to \infty} \omega_k = \sqrt{\omega_0(\omega_0 + \omega_e)}$. Nevertheless, despite this difference, if $k_{\max}$ is sufficiently large, the band gap of the original material will be virtually coincident with the band gap of the material with the cutoff (see the purple line in Fig. 3). Without the cutoff, the band gap is determined by the frequency range $\sqrt{\omega_0(\omega_0 + \omega_e)} < \omega < |\omega_0| + |\omega_e|$.

Notably, consistent with the theory of Sec. III, when a spatial-frequency cutoff is enforced the Chern numbers are always integers. The Chern numbers are calculated exactly as in Sec. III B, including the cutoff factor in the permittivity response of the material. It turns out that independent of the value $k_{\max}$ (at least for a sufficiently large $k_{\max}$), the Chern invariant for the high-frequency TM branch is $\Delta C_n = -\text{sgn}(\omega_e)$, and the Chern invariant for the low-frequency branch is $\Delta C_n = +\text{sgn}(\omega_e)$. In practice, the sign of ω_e depends on the direction of a bias magnetic field. Thus, for sufficiently large $k_{\max}$, the topology of the eigenmodes associated with the regularized material matrix is insensitive to the specific value of $k_{\max}$. This enables us to classify the material response in terms of topological invariants in an unambiguous manner.

It is interesting to see how the band structure of a material matrix of the form $\mathbf{M}_\tau(\omega,\mathbf{k}) = \mathbf{M}_\infty + \tau\chi_1(\omega,\mathbf{k}) + (1-\tau)\chi_2(\omega)$, where $0 \leqslant \tau \leqslant 1$ evolves with the parameter τ. Here, $\mathbf{M}_\infty$ represents the material matrix of the vacuum, $\chi_1(\omega,\mathbf{k}) = \mathbf{M}_1(\omega,\mathbf{k}) - \mathbf{M}_\infty$ is the susceptibility associated with the magneto-optic material of the previous example with the cutoff $k_{\max} = 3|\omega_0|/c$, and $\chi_2(\omega) = \mathbf{M}_2(\omega) - \mathbf{M}_\infty$ is the susceptibility of a lossless electric plasma defined as $\chi_2(\omega) = \begin{pmatrix} -\varepsilon_0 \frac{\omega_p^2}{\omega^2} \mathbf{1}_{3\times3} & \mathbf{0} \\ \mathbf{0} & \mathbf{0} \end{pmatrix}$ so that the plasma permittivity follows the Drude dispersion $\varepsilon_2 = \varepsilon_0(1 - \omega_p^2/\omega^2)$, where ω_p is the plasma frequency. As discussed in the beginning of this section, $\mathbf{M}_\tau(\omega,\mathbf{k})$ characterizes a well-behaved Hamiltonian for all the values of τ such that $0 \leqslant \tau \leqslant 1$. Note that $\mathbf{M}_{\tau=0}(\omega,\mathbf{k}) = \mathbf{M}_2$ and $\mathbf{M}_{\tau=1}(\omega,\mathbf{k}) = \mathbf{M}_1$.

Figure 4 shows evolution of the band structure determined by $\mathbf{M}_\tau(\omega,\mathbf{k})$ as the magneto-optic material (upper left corner) is continuously transformed into a plasma (lower right corner) with $\omega_p = 2|\omega_0|$. The first thing to note is that as the two material responses are combined (see the panels $\tau = 0.999$ and $\tau = 0.001$), an extra TM band appears in the plots. For $\tau = 0.999$, this extra band emerges as a staticlike band with $\omega \approx 0$, whereas for $\tau = 0.001$ the extra band appears as a dispersionless band with $\omega \approx |\omega_0|$. The reason for this discontinuous evolution of the band structure is that the extra band evolves into a dark mode (see Sec. II) as $\tau \to 0$ or as
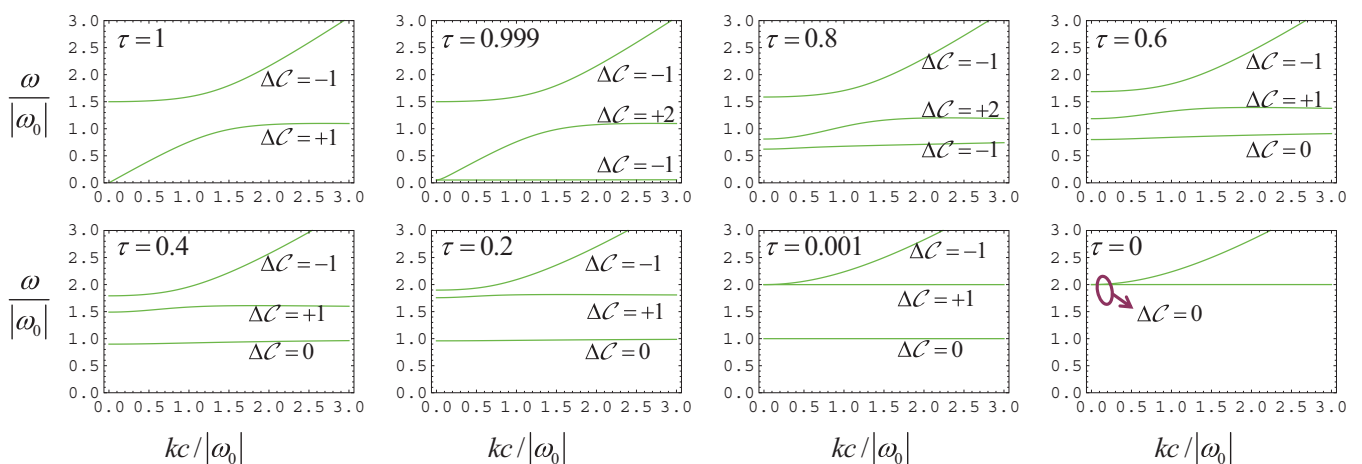

FIG. 4. (Color online) Evolution of the band structure of TM waves as a magneto-optic material ($\tau = 1$) is continuously transformed into a Drude plasma ($\tau = 0$). The magneto-optic material is characterized by the material parameters (18) with $\omega_e = 0.5\omega_0 > 0$ and a spatial cutoff $k_{\max} = 3|\omega_0|/c$, and the plasma frequency is $\omega_p = 2|\omega_0|$.
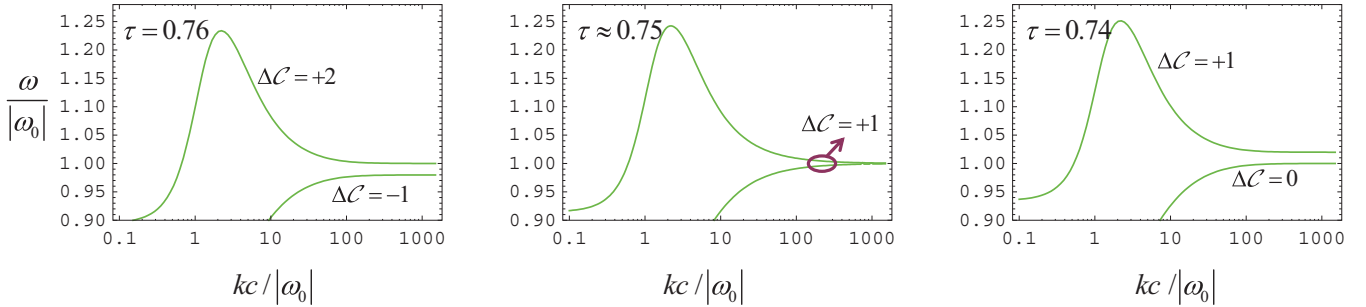
FIG. 5. (Color online) Topological transition in the vicinity $\tau \approx 0.75$. The first and second bands close and reopen at infinity (north pole) for $\tau \approx 0.75$. In this process, the Chern number associated with each band changes.

$\tau \to 1$, and hence it is not predicted by Eq. (19) when $\tau = 0$ or $\tau = 1$.

Notably, Fig. 4 reveals that for $0 \leqslant \tau < 1$ there is always a band gap between the high-frequency band and the two low-frequency bands. Moreover, in the same range, the Chern number of the high-frequency band is always $\Delta \mathcal{C} = -1$, whereas the total Chern number associated with the two low-frequency bands adds up to $+1$. Crucially, as τ becomes identical to the unity ($\tau = 1$; lower right panel of Fig. 4), the band gap between the high-frequency band and the low-frequency bands disappears. Note that in the panel with $\tau = 0.001$, a tiny but nonzero band gap persists, even though it cannot be seen at the scale of the plot. When the band gap is closed ($\tau = 1$), the Chern number of the high-frequency bands changes from $\Delta \mathcal{C} = -1$ to $\Delta \mathcal{C} = 0$. Thus, a perturbation of the material response may modify the Chern number of a given subset of bands only if the band gap is closed (and eventually reopened) in the process [23]. It should be noted that the dispersionless band that occurs at $\omega = \omega_p = 2|\omega_0|$ is associated with volume plasmons and longitudinal waves.

An eye catching feature of Fig. 4 is that the Chern number associated with the two low-frequency modes varies with τ. Particularly, it is evident that a topological transition takes place when τ varies continuously from 0.8 down to 0.6 because the Chern invariant of the second (first) band changes from $+2$ (-1) to $+1$ (0). To further investigate this topological transition, we plot in Fig. 5 with a logarithmic wave vector scale the dispersion of the first and second bands for $\tau \sim 0.75$. As seen, the first and second bands close and reopen at infinity (north pole of the Riemann sphere), and in the process the Chern numbers associated with each band changes.

As can be guessed from Fig. 4 (see panels $\tau = 1$ and $\tau = 0.999$), a similar topological transition takes place at $\tau = 1^-$ when the static dark mode becomes coupled to the electromagnetic field.

B. Edge states

Certainly the most celebrated feature of topological materials is that topologically protected edge states may appear when two topologically distinct materials with a common band gap are put side by side. The semiheuristic argument that justifies this feature is that one may regard the interface as a thin layer (with very small but finite thickness) where the Hamiltonian that characterizes one of the materials is

continuously deformed into the Hamiltonian that models the second material, similar to Fig. 4. Since the materials are topologically different, this means that in the interfacial layer the band gap needs to close (and eventually reopen) at some point. Thus, the interfacial layer may support propagating states, which may give rise to propagating modes confined to the vicinity of the interface because the adjacent materials are operated in a frequency band gap.

The edge modes supported by a generic bulk magneto-optic material and a plasma have been previously investigated [37–40]. In these seminal studies, the connection between the edge modes and the topological invariants was not made. This is done in the following.

The geometry of the relevant structure is sketched in Fig. 6 and consists of an interface (at $y = 0$) between a plasma ($y < 0$) and a magneto-optic material ($y > 0$). From Ref. [38], the dispersion equation of the TM-polarized edge modes is

$$\frac{\gamma_m}{\varepsilon_m} + \frac{\gamma_v}{\varepsilon_{ef}} = \frac{1}{\varepsilon_{ef}} \frac{\varepsilon_{12} i k_x}{\varepsilon_{11}}, \tag{30}$$

where k_x is the propagation constant of the edge state, $\varepsilon_m = 1 - \omega_p^2/\omega^2$ is the plasma permittivity, $\varepsilon_{11}, \varepsilon_{12}$ describe the permittivity response of the magneto-optic material [Eq. (18)], $\varepsilon_{ef} = \frac{\varepsilon_{11}^2 + \varepsilon_{12}^2}{\varepsilon_{11}}$, $\gamma_m = \sqrt{k_x^2 - (\omega/c)^2 \varepsilon_m}$ and $\gamma_v = \sqrt{k_x^2 - (\omega/c)^2 \varepsilon_{ef}}$.

At this point it is appropriate to recall that our theory of Chern invariants generally requires a material response with a high-frequency spatial cutoff, and hence the relevant materials are usually *nonlocal*. This creates difficulties because the electrodynamics of nonlocal media in the presence of interfaces is cumbersome and may require additional boundary conditions [27,41,42]. In practice, one may argue that if $k \ll k_{\max}$ (i.e.,
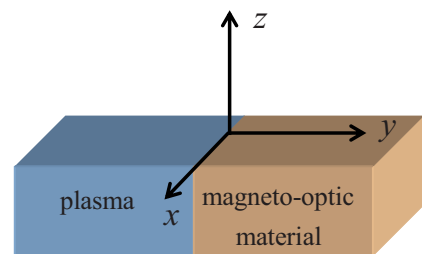

FIG. 6. (Color online) Interface between a magneto-optic material and a plasma.
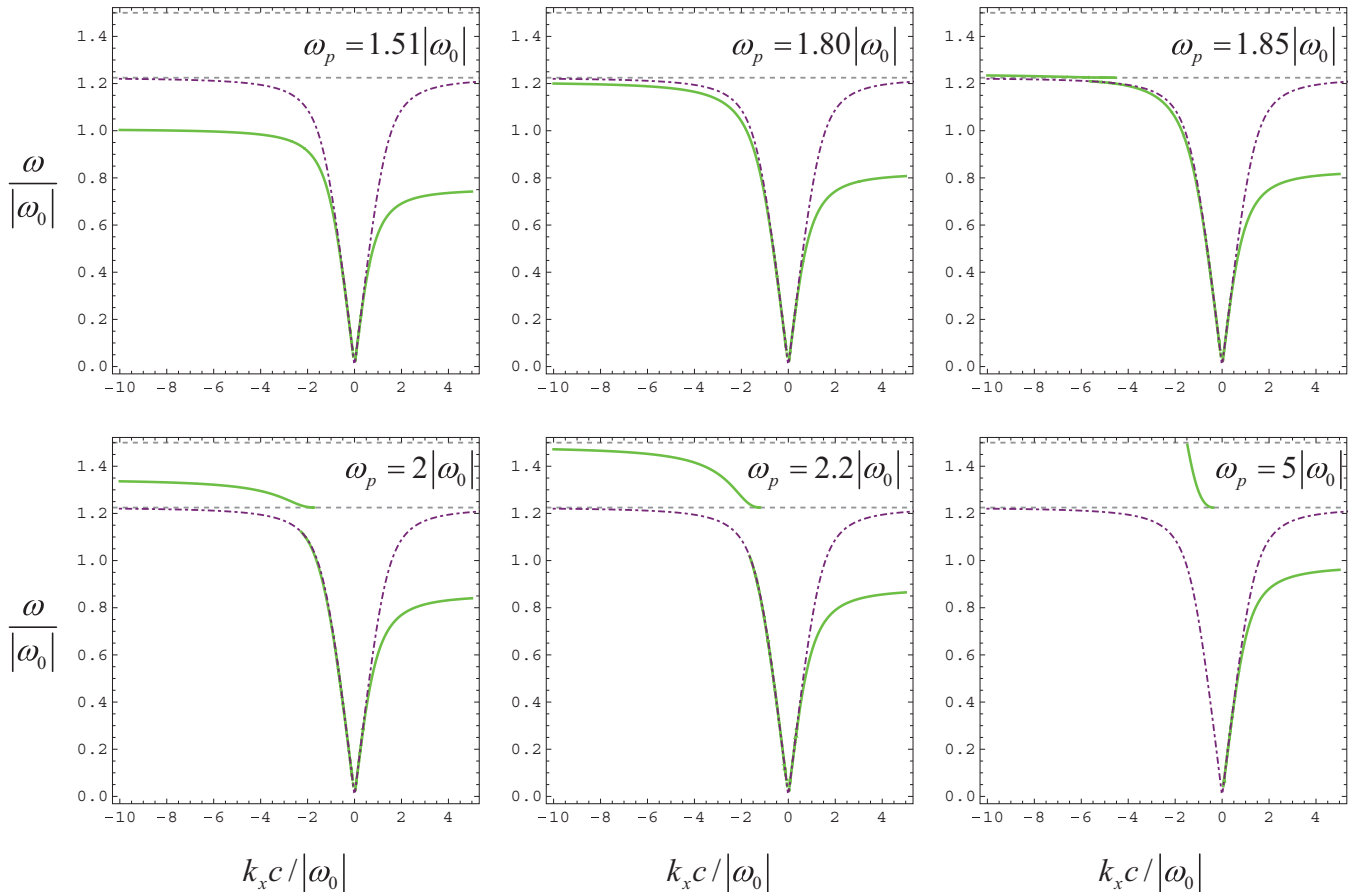
FIG. 7. (Color online) One-way edge states at an interface between a magneto-optic material and a plasma. Solid green lines: dispersion of the edge states with nonzero group velocity; purple dot-dashed lines: band structure of the magneto-optic material with material parameters given by Eq. (18) with $\omega_e = 0.5\omega_0 > 0$. The band gap is delimited by the dashed horizontal gray lines. The Drude plasma has plasma frequency ω_p.

for edge modes with $|k_x| \ll k_{\max}$), the electrodynamics of a material with a cutoff $k_{\max}$ should be essentially the same as in the material without the cutoff. Moreover, as already discussed, in the present example for a sufficiently large $k_{\max}$, the band gap of the material with the cutoff $k_{\max}$ is virtually the same as the band gap of the material without the cutoff ($k_{\max} = \infty$). Hence, these arguments show that it is acceptable to neglect the spatial cutoff when computing the dispersion of the edge modes with $|k_x| \ll k_{\max}$. Thus, in the following all the material responses are assumed local (i.e., independent of the wave vector).

Figure 7 represents the dispersion of the edge states supported by an interface between a magneto-optic material with $\omega_e = 0.5\omega_0$ and a plasma with plasma frequency ω_p. For all the examples of Fig. 7, the two materials (which are evidently topologically distinct because the plasma is topologically trivial) share a band gap defined by $1.22|\omega_0| = \sqrt{\omega_0(\omega_0 + \omega_e)} < \omega < |\omega_0| + |\omega_e| = 1.5|\omega_0|$, delimited by the dashed horizontal gray lines in the figure panels.

Notably, our results show that for ω_p below some threshold value $\omega_p < \omega_{p,th}$, there are no edge states propagating in

the band gap. For example, for $\omega_p = 1.51|\omega_0|$ the edge states (green lines in the top leftmost panel) only propagate in the frequency band associated with the first branch of the TM eigenwaves of the magneto-optic material. Interestingly, even in this regime the propagation can be highly asymmetric, and in some frequency range it can be unidirectional.

Remarkably, for $\omega_p > \omega_{p,th} \approx 1.83|\omega_0|$ the one-way edge modes emerge also within the band gap region. It can be shown that in general the plasma frequency threshold is given by $\omega_{p,th} = \sqrt{\omega_0^2 + \omega_0\omega_e + \sqrt{\omega_0(\omega_0 + \omega_e)^3}}$. At the transition $\omega_p = \omega_{p,th}$, something dramatic happens to the dispersion diagram (see the top rightmost panel): the branch associated with the edge states that propagate along the $-x$ direction is broken into two disconnected pieces. The threshold value of k_x for the upper branch (i.e., the branch within the band gap) can be found by solving $\frac{\gamma_m}{\varepsilon_m} = \frac{\varepsilon_{12}ik_x}{\varepsilon_{11}^2 + \varepsilon_{12}^2}$ with respect to k_x. This equation is obtained from the edge states dispersion (30), noting that at $\omega = \sqrt{\omega_0(\omega_0 + \omega_e)}$ (lower band gap edge), one has $\varepsilon_{ef} = \infty$. In this manner, it is found that the threshold value of k_x is given by

$$k_{x,th} = \frac{1}{c}\frac{-\sqrt{\omega_0(\omega_0 + \omega_e)^3\left(\omega_p^2 - \left(\omega_0^2 + \omega_0\omega_e\right)\right)}}{\sqrt{\left(\omega_p^2 - \left(\omega_0^2 + \omega_0\omega_e + \sqrt{\omega_0(\omega_0 + \omega_e)^3}\right)\right)\left(\omega_p^2 - \left(\omega_0^2 + \omega_0\omega_e - \sqrt{\omega_0(\omega_0 + \omega_e)^3}\right)\right)}}. \tag{31}$$
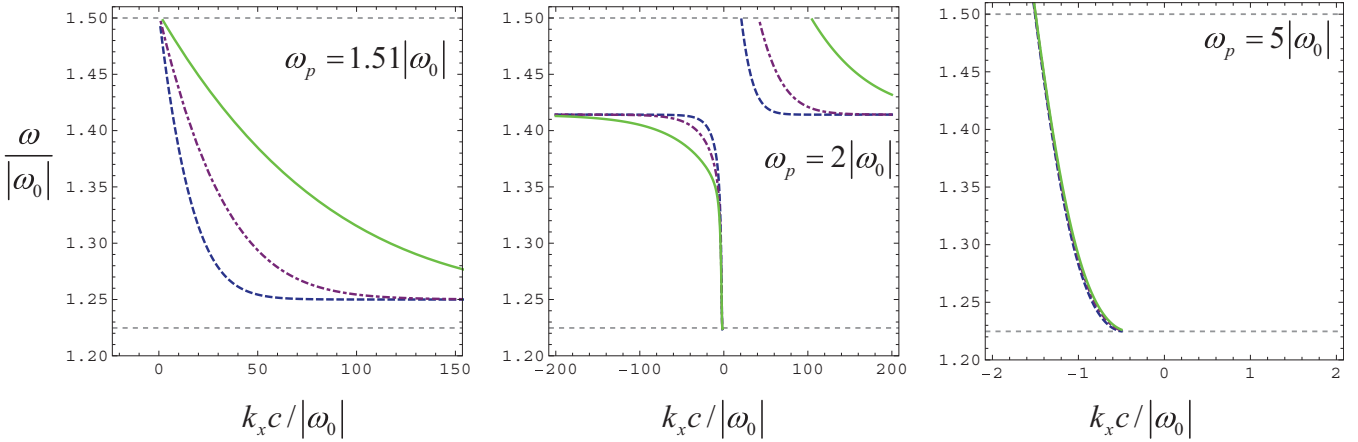
FIG. 8. (Color online) One-way edge states when a thin vacuum layer with thickness d separates the magneto-optic material and the plasma. Solid green lines: $d = 0.01c/|\omega_0|$; purple dot-dashed lines: $d = 0.025c/|\omega_0|$; blue dashed lines: $d = 0.05c/|\omega_0|$. The band gap is delimited by the dashed horizontal gray lines.

In the limit $\omega_p \to \omega_{p,th} + 0^+$, the threshold value approaches $k_{x,th} \to -\infty$. On the other hand, as $\omega_p \to +\infty$, the threshold value approaches $k_{x,th} \to 0^-$. This evolution can be seen in the sequence of panels $\omega_p = 1.85|\omega_0| \to \omega_p = 5|\omega_0|$ in Fig. 7. It should be noted that both the upper and lower branches of the edge states go suddenly into cutoff for $k_x = k_{x,th}$, and $k_x = k_{x,th}^{(2)}$, being the cutoff of the lower branch $k_{x,th}^{(2)}$ approximately (but not exactly) equal to the cutoff of the first branch $k_{x,th}$. As seen in Fig. 7, for ω_p slightly larger than $2.2|\omega_0|$, the dispersion of the one-way edge modes crosses the entire band gap of the two bulk materials. For $\omega_{p,th} < \omega_p < 2.2|\omega_0|$, the edge modes do not cross the band gap and are defined in the range $-\infty < k_x < k_{x,th}$, such that $\lim_{k_x \to -\infty} \omega_{k_x} = \omega_\infty$, where ω_∞ is some frequency in the band gap.

This example seems to indicate that the two materials may be topologically distinct and share a complete band gap but that this is insufficient to guarantee the existence of one-way edge states propagating at the interface. This appears to contradict the bulk-edge correspondence principle that links the number of edge modes with the difference of the bulk topological invariants across the interface [9,22,23]. However, it must be noted that, with exception of the case $\omega_p = 5|\omega_0|$ (more generally for $\omega_p > 2.23|\omega_0|$), in our examples the edge modes are not confined to the low-spatial frequency limit. Indeed, for $\omega_{p,th} < \omega_p < 2.23|\omega_0|$, there are edge states with arbitrarily large k_x. This suggests that for $\sqrt{\omega_0(\omega_0 + \omega_e)} < \omega_p < 2.23|\omega_0|$, it is essential to include the spatial cutoff in the material response to have a bulk-edge correspondence.

As discussed before, taking into account the spatial dispersion of the material response in the interface problem is not trivial. An approximate but simple way to introduce a spatial cutoff is to insert a thin vacuum layer (with thickness d) in between the magneto-optic material and the plasma. The justification for this is that for small values of k_x ($|k_x d| \ll 1$), the vacuum layer plays no role because the guided wavelength is much larger than the thickness of the vacuum gap. On the other hand, for large values of k_x ($|k_x d| \gg 1$), the vacuum layer mimics the spatial cutoff (27), which imposes $\lim_{k \to \infty} \mathbf{M}(\omega, \mathbf{k}) = \mathbf{M}_\infty$ being $\mathbf{M}_\infty$ the material matrix of the vacuum. Figure 8 depicts the dispersion of the edge states

that propagate in the band-gap region for different values the vacuum-layer thickness d. The details of the calculations are omitted for conciseness. The material parameters of the magneto-optic material and of the plasma are as in Fig. 7.

Comparing Figs. 7 and 8, it is seen that with the vacuum layer (i.e., with a spatial cutoff), there are always edge states in the band gap. Importantly, in the examples with $\omega_p = 1.51|\omega_0|$ and $\omega_p = 2.0|\omega_0|$, the dispersion of the edge modes tends to be more and more concentrated at high-spatial frequencies when $d \to 0^+$. This explains why some of these edge modes are not seen when $d = 0$ (Fig. 7), as the branch with $k_x > 0$ becomes effectively concentrated at $k = \infty$ ($\omega_p = 2.0|\omega_0|$) or moves toward the upper band gap edge ($\omega_p = 1.51|\omega_0|$). In contrast, the edge states associated with $\omega_p = 5.0|\omega_0|$ are virtually independent of d and are associated with low-spatial frequencies. Hence, consistent with theory developed in Sec. III, to have a bulk-edge correspondence it seems essential to include the high-spatial frequency cutoff in the analysis.

V. CONCLUSION

It was demonstrated that notwithstanding that the underlying wave vector space is open and unbounded it is possible to calculate Chern invariants of a wide class of well-behaved continuous media described by a bianisotropic spatially dispersive material matrix. Generally, a local material—with effective parameters independent of the wave vector—does not belong to this class. However, the response of a local material can be arbitrarily well approximated by that an element of the subclass of well-behaved Hamiltonians. We explicitly constructed such a Hamiltonian by introducing a spatial cutoff $k_{\max}$ in the local material response. In principle, the Chern invariant is independent of the considered cutoff when $k_{\max}$ in Eq. (15) is sufficiently large. Thus, the proposed theory enables us to topologically classify continuous media and gives important insights on the emergence of edge states at interfaces of topologically inequivalent continuous materials. We hope that the proposed ideas may contribute to deepen the understanding of topological photonics and to further develop this subject.

APPENDIX A: PARTIAL FRACTION DECOMPOSITION OF THE MATERIAL MATRIX

In this Appendix, it is shown that the material matrix $\mathbf{M} = \mathbf{M}(\omega, \mathbf{k})$ of a dispersive lossless material may be written for ω in the real-frequency axis as

$$\mathbf{M}(\omega, \mathbf{k}) = \mathbf{M}_\infty - \sum_\alpha \frac{\mathrm{sgn}(\omega_{p,\alpha})}{\omega - \omega_{p,\alpha}} \mathbf{A}_\alpha^2, \qquad (A1)$$

with $\mathbf{A}_\alpha = [-\mathrm{sgn}(\omega_{p,\alpha})(\mathrm{Res}\mathbf{M})_\alpha]^{1/2} \geqslant 0$, i.e., $\mathbf{A}_\alpha$ is a positive (semi-)definite matrix. In the above, $\mathrm{sgn} = \pm$ is the sign of a real number, $\mathbf{M}_\infty = \lim_{\omega \to \infty} \mathbf{M}(\omega, \mathbf{k})$, $\omega_{p,\alpha}$ are the (real-valued) poles of the frequency response, $(\mathrm{Res}\mathbf{M})_\alpha$ represents the corresponding residue, and the wave vector $\mathbf{k}$ is real valued. An immediate consequence of Eq. (A1) is that

$$\frac{\partial}{\partial \omega}[\omega \mathbf{M}(\omega, \mathbf{k})] = \mathbf{M}_\infty + \sum_\alpha \frac{|\omega_{p,\alpha}|\mathbf{A}_\alpha^2}{(\omega - \omega_{p,\alpha})^2}. \qquad (A2)$$

To simplify the notations, in what follows the dependence of $\mathbf{M}$ on $\mathbf{k}$ is omitted.

To prove Eq. (A1), we start by noting that due to the causality of the material response, the matrix $\mathbf{M}$ is required to be an analytic function of ω in the upper-half frequency plane ($\mathrm{Im}\{\omega\} > 0$) for any fixed $\mathbf{k}$ [26,27]. In particular, $\mathbf{M}$ does not have any poles in the upper-half plane. Hence, from Cauchy's theorem we can state that $0 = \frac{1}{2\pi i} \oint_C \frac{\mathbf{M}(\Omega) - \mathbf{M}_\infty}{\Omega - \omega} d\Omega$, where C is a closed contour contained in the semiplane $\mathrm{Im}\{\Omega\} \geqslant 0$, and it is assumed that ω is in the real axis and is exterior to C. We take C as the contour that consists of the real axis (excluding the poles of the integrand, $\omega_{p,\alpha}$, $\alpha = 1,2,...,$ and ω) and a semicircle of infinite radius in the upper-half plane. In the vicinity of a given pole, the contour C consists of a semicircle of infinitesimal radius contained in the upper-half plane. Assuming that the material response decays sufficiently fast at infinity and calculating the integrals over the semicircles around the poles, it is found that

$$0 = \frac{1}{2\pi i}\mathrm{P.V.} \int \frac{\mathbf{M}(\Omega) - \mathbf{M}_\infty}{\Omega - \omega} d\Omega + \frac{1}{2\pi i}(-\pi i)\sum_\alpha \frac{(\mathrm{Res}\mathbf{M})_\alpha}{\omega_{p,\alpha} - \omega}$$
$$+ \frac{1}{2\pi i}(-\pi i)[\mathbf{M}(\omega) - \mathbf{M}_\infty], \qquad (A3)$$

where P.V. denotes the principal value of the integral over the real axis and $(\mathrm{Res}\mathbf{M})_\alpha$ is the residue associated with the pole $\omega_{p,\alpha}$. Note that for spatially dispersive media, $\omega_{p,\alpha}$ and $(\mathrm{Res}\mathbf{M})_\alpha$ may depend on the wave vector. The obtained result can be rewritten as

$$\mathbf{M}(\omega) - \mathbf{M}_\infty = \frac{1}{\pi i}\mathrm{P.V.} \int \frac{\mathbf{M}(\Omega) - \mathbf{M}_\infty}{\Omega - \omega} d\Omega + \sum_\alpha \frac{(\mathrm{Res}\mathbf{M})_\alpha}{\omega - \omega_{p,\alpha}}. \qquad (A4)$$

Importantly, for ω in the real axis and lossless media, the material matrix is required to satisfy $\mathbf{M} = \mathbf{M}^\dagger$ [Eq. (4)]. This

implies that the integral over the real axis vanishes, and hence we obtain the following partial fraction decomposition of the material matrix:

$$\mathbf{M}(\omega) = \mathbf{M}_\infty - \sum_\alpha \frac{\mathbf{B}_\alpha}{\omega - \omega_{p,\alpha}}, \quad \mathbf{B}_\alpha = -(\mathrm{Res}\mathbf{M})_\alpha. \quad (A5)$$

From here, it follows that

$$\frac{\partial}{\partial \omega}[\omega \mathbf{M}(\omega)] = \mathbf{M}_\infty + \sum_\alpha \frac{\omega_{p,\alpha}\mathbf{B}_\alpha}{(\omega - \omega_{p,\alpha})^2}. \qquad (A6)$$

As discussed in the main text, $\frac{\partial}{\partial \omega}[\omega \mathbf{M}(\omega)]$ is required to be positive definite [Eq. (5)]. This is only possible if $\mathbf{B}_\alpha \mathrm{sgn}(\omega_{p,\alpha}) \geqslant 0$; that is, $\mathbf{B}_\alpha \mathrm{sgn}(\omega_{p,\alpha})$ must be non-negative. Therefore, it is possible to write

$$\mathbf{B}_\alpha = \mathrm{sgn}(\omega_{p,\alpha})\mathbf{A}_\alpha^2, \qquad (A7)$$

with $\mathbf{A}_\alpha = [\mathrm{sgn}(\omega_{p,\alpha})\mathbf{B}_\alpha]^{1/2} \geqslant 0$, which is a (semi-)positive definite Hermitian matrix. Substituting this result into Eq. (A5), we readily obtain the desired result [Eq. (A1)].

APPENDIX B: THE GENERALIZED ELECTROMAGNETIC PROBLEM

Let us consider a dispersive material characterized by the material matrix $\mathbf{M} = \mathbf{M}(\omega, \mathbf{k})$. In the spectral domain ($\partial_t \leftrightarrow -i\omega$ and $\nabla \leftrightarrow i\mathbf{k}$), Maxwell's equations (1) are equivalent to

$$\hat{N} \cdot \mathbf{f} = \omega \mathbf{M}(\omega, \mathbf{k}) \cdot \mathbf{f} + i\mathbf{j}, \quad \text{with}$$
$$\hat{N} = \begin{pmatrix} \mathbf{0} & -\mathbf{k} \times \mathbf{1}_{3\times3} \\ \mathbf{k} \times \mathbf{1}_{3\times3} & \mathbf{0} \end{pmatrix}. \qquad (B1)$$

The objective of this Appendix is to obtain a formalism equivalent to (B1) but with the time dynamics determined by a first-order in time partial differential system [Eq. (7) of the main text], analogous to the Schrödinger equation. With this purpose, we introduce the auxiliary fields

$$\mathbf{Q}_\alpha = \frac{|\omega_{p,\alpha}|^{1/2}}{(\omega - \omega_{p,\alpha})} \mathbf{A}_\alpha \cdot \mathbf{f}, \quad \alpha = 1,2,..., \qquad (B2)$$

where $\omega_{p,\alpha}$ and $\mathbf{A}_\alpha$ are defined as in Appendix A and in general may depend on the wave vector $\mathbf{k}$. Evidently, one may write

$$\omega \mathbf{Q}_\alpha = \omega_{p,\alpha} \mathbf{Q}_\alpha + |\omega_{p,\alpha}|^{1/2} \mathbf{A}_\alpha \cdot \mathbf{f}. \qquad (B3)$$

Using the partial-fraction decomposition of the material matrix (A1), it is found that

$$\mathbf{g} = \mathbf{M} \cdot \mathbf{f} = \mathbf{M}_\infty \cdot \mathbf{f} - \sum_\alpha \mathrm{sgn}(\omega_{p,\alpha}) \frac{1}{|\omega_{p,\alpha}|^{1/2}} \mathbf{A}_\alpha \cdot \mathbf{Q}_\alpha. \qquad (B4)$$

Hence, from Eq. (B3), we get

$$\omega \mathbf{g} = \omega \mathbf{M}_\infty \cdot \mathbf{f} - \sum_\alpha \mathrm{sgn}(\omega_{p,\alpha}) \frac{1}{|\omega_{p,\alpha}|^{1/2}} \mathbf{A}_\alpha$$
$$\cdot [\omega_{p,\alpha} \mathbf{Q}_\alpha + |\omega_{p,\alpha}|^{1/2} \mathbf{A}_\alpha \cdot \mathbf{f}]$$
$$= \omega \mathbf{M}_\infty \cdot \mathbf{f} - \sum_\alpha |\omega_{p,\alpha}|^{1/2} \mathbf{A}_\alpha \cdot \mathbf{Q}_\alpha - \sum_\alpha \mathrm{sgn}(\omega_{p,\alpha}) \mathbf{A}_\alpha^2 \cdot \mathbf{f}. \qquad (B5)$$

Thus, substituting this formula into Maxwell's equations (B1) and calculating the inverse Fourier transform in time of the resulting equation and of Eq. (B3), we obtain the desired first-order in time partial differential system:

$$
\left(\hat{N} + \sum_\alpha \mathrm{sgn}(\omega_{p,\alpha}) \mathbf{A}_\alpha^2 \right) \cdot \mathbf{f} + \sum_\alpha |\omega_{p,\alpha}|^{1/2} \mathbf{A}_\alpha \cdot \mathbf{Q}_\alpha
$$

$$
= i \frac{\partial}{\partial t} \mathbf{M}_\infty \cdot \mathbf{f} + i \mathbf{j}, \tag{B6a}
$$

$$
|\omega_{p,\alpha}|^{1/2} \mathbf{A}_\alpha \cdot \mathbf{f} + \omega_{p,\alpha} \mathbf{Q}_\alpha = i \frac{\partial}{\partial t} \mathbf{Q}_\alpha. \tag{B6b}
$$

Notably, this set of equations can be written in a matrix form, $\hat{L} \cdot \mathbf{Q} = i \frac{\partial}{\partial t} \mathbf{M}_g \cdot \mathbf{Q} + i \mathbf{j}_g$, with the relevant symbols defined as in Eq. (7) in the main text. Because $\mathbf{A}_\alpha$ and $\mathbf{M}_\infty$

are Hermitian matrices, it is easy to check that the operators $\hat{L}$ and $\mathbf{M}_g$ are also Hermitian with respect to the canonical inner product. This implies that for a fixed $\mathbf{k}$, the operator $\hat{H}_{cl} = \mathbf{M}_g^{-1} \cdot \hat{L}$ is Hermitian with respect to the weighted inner product (9).

In order to demonstrate Eq. (10) in the main text, let us consider now two generic solutions, $\mathbf{Q}_A(\mathbf{r},t) = \tilde{\mathbf{Q}}_A e^{-i\omega_A t} e^{i\mathbf{k}\cdot\mathbf{r}}$ and $\mathbf{Q}_B(\mathbf{r},t) = \tilde{\mathbf{Q}}_B e^{-i\omega_B t} e^{i\mathbf{k}\cdot\mathbf{r}}$ of the generalized problem [Eq. (7)], with a space-time dependence of the form $e^{-i\omega t} e^{i\mathbf{k}\cdot\mathbf{r}}$. Note that the wave vector is the same for both fields, but the frequency ω may be different. The fields $\mathbf{Q}_A$ and $\mathbf{Q}_B$ are not necessarily natural modes of the system and may be associated with some external current excitations, $\mathbf{j}_A$ and $\mathbf{j}_B$, respectively. The envelopes of the generalized state variables are $\tilde{\mathbf{Q}}_A$ and $\tilde{\mathbf{Q}}_B$. Let $\mathbf{f}_A(\mathbf{r},t) = \mathbf{F}_A e^{-i\omega_A t} e^{i\mathbf{k}\cdot\mathbf{r}}$ and $\mathbf{f}_B(\mathbf{r},t) = \mathbf{F}_B e^{-i\omega_B t} e^{i\mathbf{k}\cdot\mathbf{r}}$ be the corresponding solutions of Maxwell's equations (B1). Then, from Eq. (B2) it is straightforward to verify that

$$
\frac{1}{2} \tilde{\mathbf{Q}}_B^* \cdot \mathbf{M}_g \cdot \tilde{\mathbf{Q}}_A = \frac{1}{2} \left[\mathbf{F}_B^* \cdot \mathbf{M}_\infty \cdot \mathbf{F}_A + \mathbf{F}_B^* \cdot \sum_\alpha \mathbf{A}_\alpha \frac{|\omega_{p,\alpha}|^{1/2}}{(\omega_B - \omega_{p,\alpha})} \cdot \frac{|\omega_{p,\alpha}|^{1/2}}{(\omega_A - \omega_{p,\alpha})} \mathbf{A}_\alpha \cdot \mathbf{F}_A \right], \tag{B7}
$$

where $\mathbf{M}_g$ is defined as in Eq. (7). Using Eq. (A1), it is possible write the above result in a rather compact manner:

$$
\frac{1}{2} \tilde{\mathbf{Q}}_B^* \cdot \mathbf{M}_g \cdot \tilde{\mathbf{Q}}_A = \frac{1}{2} \mathbf{F}_B^* \cdot \left[\frac{\omega_B \mathbf{M}(\omega_B,\mathbf{k}) - \omega_A \mathbf{M}(\omega_A,\mathbf{k})}{\omega_B - \omega_A} \right] \cdot \mathbf{F}_A. \tag{B8}
$$

In particular, in the limit $\omega_B = \omega_A \equiv \omega$ (it is always possible to take this limit because $\mathbf{Q}_A$ and $\mathbf{Q}_B$ are generally driven by external excitations $\mathbf{j}_A$ and $\mathbf{j}_B$), it is found that

$$
\frac{1}{2} \mathbf{Q}_B^* \cdot \mathbf{M}_g \cdot \mathbf{Q}_A = \frac{1}{2} \mathbf{f}_B^* \cdot \frac{\partial}{\partial \omega} [\omega \mathbf{M}(\omega,\mathbf{k})] \cdot \mathbf{f}_A. \tag{B9}
$$

Choosing $\mathbf{Q}_A = \mathbf{Q}_B \equiv \mathbf{Q}$, one finally obtains Eq. (10) of the main text.

APPENDIX C: THE BERRY POTENTIAL ASSOCIATED WITH THE GENERALIZED PROBLEM

In what follows, we derive the conditions under which the identity [Eq. (14)] is valid. To this end, we substitute Eq. (B2) into the definition of the Berry potential [Eq. (13)] to obtain

$$
\mathcal{A}_{n\mathbf{k}} = \frac{1}{2} i \mathbf{f}_{n\mathbf{k}}^* \cdot \mathbf{M}_\infty \cdot \partial_\mathbf{k} \mathbf{f}_{n\mathbf{k}} + \frac{1}{2} i \mathbf{f}_{n\mathbf{k}}^* \cdot \sum_\alpha \mathbf{A}_{\alpha,\mathbf{k}} \frac{|\omega_{p,\alpha,\mathbf{k}}|^{1/2}}{(\omega_{n\mathbf{k}} - \omega_{p,\alpha,\mathbf{k}})} \partial_\mathbf{k} \left[\mathbf{A}_{\alpha,\mathbf{k}} \frac{|\omega_{p,\alpha,\mathbf{k}}|^{1/2}}{(\omega_{n\mathbf{k}} - \omega_{p,\alpha,\mathbf{k}})} \cdot \mathbf{f}_{n\mathbf{k}} \right]. \tag{C1}
$$

In the above formula, we indicate explicitly the possible dependence of $\mathbf{A}_{\alpha,\mathbf{k}}$ and $\omega_{p,\alpha,\mathbf{k}}$ on the wave vector and assumed that $\mathbf{M}_\infty$ is independent of $\mathbf{k}$. Using Eq. (A2), the Berry potential can be rewritten as

$$
\mathcal{A}_{n\mathbf{k}} = \frac{1}{2} i \mathbf{f}_{n\mathbf{k}}^* \cdot \frac{\partial}{\partial \omega} [\omega \mathbf{M}(\omega,\mathbf{k})]_{\omega_{n\mathbf{k}}} \cdot \partial_\mathbf{k} \mathbf{f}_{n\mathbf{k}} + \frac{1}{2} i \mathbf{f}_{n\mathbf{k}}^* \cdot \sum_\alpha \mathbf{A}_{\alpha,\mathbf{k}} \frac{|\omega_{p,\alpha,\mathbf{k}}|^{1/2}}{(\omega_{n\mathbf{k}} - \omega_{p,\alpha,\mathbf{k}})} \partial_\mathbf{k} \left[\mathbf{A}_{\alpha,\mathbf{k}} \frac{|\omega_{p,\alpha,\mathbf{k}}|^{1/2}}{(\omega_{n\mathbf{k}} - \omega_{p,\alpha,\mathbf{k}})} \right] \cdot \mathbf{f}_{n\mathbf{k}}. \tag{C2}
$$

Taking into account that $\mathcal{A}_{n\mathbf{k}}$ is real valued and that $\mathbf{A}_{\alpha,\mathbf{k}}$ is Hermitian, it follows that

$$
\mathcal{A}_{n\mathbf{k}} = \mathrm{Re}\left\{ \frac{1}{2} i \mathbf{f}_{n\mathbf{k}}^* \cdot \frac{\partial}{\partial \omega} [\omega \mathbf{M}(\omega,\mathbf{k})]_{\omega_{n\mathbf{k}}} \cdot \partial_\mathbf{k} \mathbf{f}_{n\mathbf{k}} + \frac{1}{2} i \mathbf{f}_{n\mathbf{k}}^* \cdot \sum_\alpha \frac{|\omega_{p,\alpha,\mathbf{k}}|}{(\omega_{n\mathbf{k}} - \omega_{p,\alpha,\mathbf{k}})^2} (\mathbf{A}_{\alpha,\mathbf{k}} \cdot \partial_\mathbf{k} \mathbf{A}_{\alpha,\mathbf{k}}) \cdot \mathbf{f}_{n\mathbf{k}} \right\}
$$

$$
= \mathrm{Re}\left\{ \frac{1}{2} i \mathbf{f}_{n\mathbf{k}}^* \cdot \frac{\partial}{\partial \omega} [\omega \mathbf{M}(\omega,\mathbf{k})]_{\omega_{n\mathbf{k}}} \cdot \partial_\mathbf{k} \mathbf{f}_{n\mathbf{k}} \right\} + \frac{1}{2} \mathbf{f}_{n\mathbf{k}}^* \cdot \tilde{\mathbf{M}}(\omega_{n\mathbf{k}},\mathbf{k}) \cdot \mathbf{f}_{n\mathbf{k}}, \tag{C3}
$$

where we defined

$$
\tilde{\mathbf{M}}(\omega,\mathbf{k}) = i \sum_\alpha \frac{|\omega_{p,\alpha,\mathbf{k}}|}{(\omega - \omega_{p,\alpha,\mathbf{k}})^2} \frac{1}{2} [\mathbf{A}_{\alpha,\mathbf{k}}, \partial_\mathbf{k} \mathbf{A}_{\alpha,\mathbf{k}}], \tag{C4}
$$

and $[\mathbf{A}_{\alpha,\mathbf{k}}, \partial_{\mathbf{k}}\mathbf{A}_{\alpha,\mathbf{k}}] = \mathbf{A}_{\alpha,\mathbf{k}} \cdot \partial_{\mathbf{k}}\mathbf{A}_{\alpha,\mathbf{k}} - \partial_{\mathbf{k}}\mathbf{A}_{\alpha,\mathbf{k}} \cdot \mathbf{A}_{\alpha,\mathbf{k}}$ stands for the commutator of the two operators. It should be noted that $\tilde{\mathbf{M}}(\omega,\mathbf{k})$ represents a pair of Hermitian matrices: one matrix is associated with the derivative along the k_x direction ($\hat{\mathbf{x}} \cdot \partial_{\mathbf{k}}$) and determines the component $\mathcal{A}_{n\mathbf{k}} \cdot \hat{\mathbf{x}}$ of the Berry potential, whereas the second matrix depends on the derivative along the k_y direction and determines $\mathcal{A}_{n\mathbf{k}} \cdot \hat{\mathbf{y}}$. It does not seem possible to further simplify Eq. (C3) without further assumptions.

Next, we examine the case wherein the matrices $\mathbf{A}_{\alpha,\mathbf{k}}$ have a dependence on $\mathbf{k}$ of the form

$$\mathbf{A}_{\alpha,\mathbf{k}} = c_{\mathbf{k}}\mathbf{A}_{\alpha,0} \tag{C5}$$

where $\mathbf{A}_{\alpha,0}$ is a constant matrix and $c_{\mathbf{k}}$ is some scalar function of the wave vector. It is immediate to check that in such circumstances $[\mathbf{A}_{\alpha,\mathbf{k}}, \partial_{\mathbf{k}}\mathbf{A}_{\alpha,\mathbf{k}}] = 0$, and hence $\tilde{\mathbf{M}}(\omega,\mathbf{k})$ vanishes. Hence, for such a subclass of spatially dispersive media the Berry potential is given by the formula of Raghu and Haldane [Eq. (14)].

Let us study now the interesting situation wherein the material matrix satisfies Eq. (15). Clearly, the residues of the material matrix are of the form $-(\mathrm{Res}\mathbf{M})_{\alpha,\mathbf{k}} = \frac{1}{1+k^2/k_{\max}^2}\mathbf{B}_{\alpha,0}$, where $\mathbf{B}_{\alpha,0}$ is independent of the wave vector. Taking into account that $\mathbf{A}_{\alpha,\mathbf{k}} = [-\mathrm{sgn}(\omega_{p,\alpha,\mathbf{k}})(\mathrm{Res}\mathbf{M})_{\alpha,\mathbf{k}}]^{1/2}$ (see Appendix A), it is evident that $\mathbf{A}_{\alpha,\mathbf{k}}$ satisfies Eq. (C5). This confirms that the Berry potential associated with the subclass of spatially dispersive media with a response as in Eq. (15) can be computed using the formula of Raghu and Haldane [Eq. (14)].

Returning again to the general case in Eq. (C3), it is relevant to note that the second addend in the rightmost identity of this equation is always Gauge invariant. Thus, in principle this second term is free of singularities in the $\mathbf{k}$ plane. If this term also decays sufficiently fast at infinity then from Stoke's theorem, its integral over the Riemann sphere vanishes. In such a case, the second addend can be ignored in the calculation of the Chern number, and one recovers again the result in Eq. (14).

APPENDIX D: THE BERRY POTENTIAL IN THE RIEMANN SPHERE

Here, we discuss how to define the Berry potential over the Riemann sphere. To this end we recall that the stereographic projection (17) defines a one-to-one mapping of the $\mathbf{k}$ plane plus infinity onto the Riemann sphere $(k_x,k_y) \to \kappa$. Thus, the electromagnetic field envelope $\mathbf{f}_{n\mathbf{k}}$ may be seen as a function of κ, i.e., may be regarded as being defined over the Riemann

sphere. Hence, the Berry potential in the Riemann sphere is given by (compare with the corresponding definition (14) in the plane)

$$\mathcal{A}_{RS,\kappa} = \mathrm{Re}\left\{ i\,\mathbf{f}_{n\mathbf{k}}^* \cdot \frac{1}{2}\frac{\partial}{\partial\omega}[\omega\mathbf{M}(\omega,\mathbf{k})]_{\omega_{n\mathbf{k}}} \cdot \mathrm{Grad}_{\kappa}\mathbf{f}_{n\mathbf{k}} \right\}. \tag{D1}$$

In the above formula, Grad_{κ} is the surface gradient [43], and $\mathbf{k}$ is understood as a function of κ determined by the inverse stereographic projection $(k_x,k_y) = (\kappa_x,\kappa_y)\frac{1}{1-\kappa_z}$. Using the surface gradient definition [43], it is possible to prove that (the symbol $\otimes$ stands for the tensor product of two vectors)

$$\mathcal{A}_{RS,\kappa} = \frac{1}{\sqrt{E}}\mathcal{A}_{\mathbf{k}} \cdot (\hat{\mathbf{x}} \otimes \hat{\mathbf{t}}_x + \hat{\mathbf{y}} \otimes \hat{\mathbf{t}}_y), \tag{D2}$$

with $\hat{\mathbf{t}}_i = \frac{\partial\kappa}{\partial k_i}/|\frac{\partial\kappa}{\partial k_i}|$ $(i = x,y)$ and $E = \frac{\partial\kappa}{\partial k_x} \cdot \frac{\partial\kappa}{\partial k_x} = \frac{\partial\kappa}{\partial k_y} \cdot \frac{\partial\kappa}{\partial k_y} = \frac{4}{(k^2+1)^2}$. Here, $\frac{\partial\kappa}{\partial k_i}$ is determined using the stereographic projection (17). Note that $\hat{\mathbf{t}}_x$ and $\hat{\mathbf{t}}_y$ form an orthonormal basis of the tangent space in each point of the Riemann sphere, and thus $\mathcal{A}_{RS,\kappa}$ is tangent to the spherical surface with unit radius. The Berry curvature in the Riemann sphere is defined as

$$\mathcal{F}_{RS,\kappa} = \mathrm{Div}(\hat{\mathbf{n}} \times \mathcal{A}_{RS,\kappa}), \tag{D3}$$

where $\hat{\mathbf{n}}$ is the outward unit vector normal to the sphere surface and Div stands for the surface divergence operator [43]. Taking into account that if $\mathbf{B} = b_1\frac{\partial\kappa}{\partial k_1} + b_2\frac{\partial\kappa}{\partial k_2}$, then $\mathrm{Div}\mathbf{B} = \frac{1}{E}\frac{\partial}{\partial k_1}(Eb_1) + \frac{1}{E}\frac{\partial}{\partial k_2}(Eb_2)$ [43] and that $\hat{\mathbf{t}}_x \times \hat{\mathbf{t}}_y = -\hat{\mathbf{n}}$ it is easily found that

$$\mathcal{F}_{RS,\kappa} = \frac{1}{E}\mathcal{F}_{\mathbf{k}}, \tag{D4}$$

where $\mathcal{F}_{\mathbf{k}} = \frac{\partial\mathcal{A}_x}{\partial k_y} - \frac{\partial\mathcal{A}_y}{\partial k_x}$ is the Berry curvature in the plane. The Chern number is the integral of the Berry curvature in the sphere

$$\mathcal{C}_{RS} = \frac{1}{2\pi}\iint_{RS} ds\, \mathcal{F}_{RS,\kappa}. \tag{D5}$$

Since the element of area in the sphere's surface is $ds = E\,dk_x\,dk_y$ it is finally found that

$$\mathcal{C}_{RS} = \frac{1}{2\pi}\int_{-\infty}^{+\infty}\int_{-\infty}^{+\infty} dk_x dk_y \mathcal{F}_{\kappa} = \mathcal{C}, \tag{D6}$$

i.e., the Chern number in the Riemann sphere can be calculated using the Berry curvature defined in the plane [Eq. (16)].

[1] E. Yablonovitch, Inhibited Spontaneous Emission in Solid-State Physics and Electronics, Phys. Rev. Lett. **58**, 2059 (1987).

[2] J. D. Joannopoulos, S. G. Johnson, J. N. Winn, and R. D. Meade, *Photonic Crystals: Molding the Flow of Light*, 2nd ed. (Princeton University Press, New Jersey, 2008).

[3] A. F. Koenderink, A. Alù, and A. Polman, Nanophotonics: Shrinking light-based technology, Science **348**, 516 (2015).

[4] H. Kosaka, T. Kawashima, A. Tomita, M. Notomi, T. Tamamura, T. Sato, and S. Kawakami, Superprism phenomena in photonic crystals, Phys. Rev. B **58**, R10096(R) (1998).

[5] C. Luo, S. G. Johnson, J. D. Joannopoulos, and J. B. Pendry, Subwavelength imaging in photonic crystals, Phys. Rev. B **68**, 045115 (2003).

[6] N. Engheta and R. W. Ziolkowski, *Metamaterials: Physics and Engineering Explorations* (Wiley-IEEE Press, Hoboken, NJ, 2006).

[7] F. D. M. Haldane and S. Raghu, Possible Realization of Directional Optical Waveguides in Photonic Crystals with Broken Time-Reversal Symmetry, Phys. Rev. Lett. **100**, 013904 (2008).

[8] S. Raghu and F. D. M. Haldane, Analogs of quantum-Hall-effect edge states in photonic crystals, Phys. Rev. A **78**, 033834 (2008).

[9] L. Lu, J. D. Joannopoulos, and M. Soljačić, Topological photonics, Nat. Photonics **8**, 821 (2014).

[10] Z. Wang, Y. D. Chong, J. D. Joannopoulos, and M. Soljačić, Reflection-Free One-Way Edge Modes in a Gyromagnetic Photonic Crystal, Phys. Rev. Lett. **100**, 013905 (2008).

[11] Z. Yu, G. Veronis, Z. Wang, and S. Fan, One-Way Electromagnetic Waveguide Formed at the Interface Between a Plasmonic Metal Under a Static Magnetic Field and a Photonic Crystal, Phys. Rev. Lett. **100**, 023902 (2008).

[12] Z. Wang, Y. Chong, J. D. Joannopoulos, and M. Soljačić, Observation of unidirectional backscattering immune topological electromagnetic states, Nature **461**, 772 (2009).

[13] Y. Poo, R.-X. Wu, Z. Lin, Y. Yang, and C.T. Chan, Experimental Realization of Self-Guiding Unidirectional Electromagnetic Edge States, Phys. Rev. Lett. **106**, 093903 (2011).

[14] W. Qiu, Z. Wang, and M. Soljačić, Broadband circulators based on directional coupling of one-way waveguides, Optics Express **19**, 22248 (2011).

[15] M. C. Rechtsman, J. M. Zeuner, Y. Plotnik, Y. Lumer, D. Podolsky, F. Dreisow, S. Nolte, M. Segev, and A. Szameit, Photonic Floquet topological insulators, Nature **496**, 196 (2013).

[16] Y. Lumer, Y. Plotnik, M. C. Rechtsman, and M. Segev, Self-Localized States in Photonic Topological Insulators, Phys. Rev. Lett. **111**, 243905 (2013).

[17] M. P. do Carmo, *Differential Geometry of Curves and Surfaces* (Prentice-Hall, Englewood Cliffs, NJ, 1976).

[18] D. J. Thouless, M. Kohmoto, M. P. Nightingale, and M. den Nijs, Quantized Hall Conductance in a Two-Dimensional Periodic Potential, Phys. Rev. Lett. **49**, 405 (1982).

[19] B. Simon, Holonomy, the Quantum Adiabatic Theorem, and Berry's Phase, Phys. Rev. Lett. **51**, 2167 (1983).

[20] A. B. Khanikaev, S. H. Mousavi, W.-K. Tse, M. Kargarian, A. H. MacDonald, and G. Shvets, Photonic topological insulators, Nat. Materials **12**, 233 (2013).

[21] L.-H. Wu and X. Hu, Scheme for Achieving a Topological Photonic Crystal by Using Dielectric Material, Phys. Rev. Lett. **114**, 223901 (2015).

[22] M. Z. Hasan and C. L. Kane, Colloquium: Topological insulators, Rev. Mod. Phys. **82**, 3045 (2010).

[23] B. A. Bernervig and T. Hughes, *Topological Insulators and Topological Superconductors* (Princeton University Press, New Jersey, 2013).

[24] I. V. Lindell, A. H. Sihvola, S. A. Tretyakov, and A. J. Viitanen, *Electromagnetic Waves in Chiral and Bi-Isotropic Media* (Artech House, Boston, Massachusetts, 1994).

[25] A. Serdyukov, I. Semchenko, S. Tretyakov, and A. Sihvola, *Electromagnetics of Bianisotropic Materials Theory and Applications*, 1st ed. (Gordon and Breach Science Publishers, Amsterdam, 2001).

[26] L. D. Landau and E. M. Lifshitz, *Electrodynamics of Continuous Media*, Course of Theoretical Physics, Vol. 8 (Elsevier Butterworth-Heinemann, Oxford, UK, 2004).

[27] V. Agranovich and V. Ginzburg, *Spatial Dispersion in Crystal Optics and the Theory of Excitons* (Wiley-Interscience, New York, 1966).

[28] M. G. Silveirinha and S. I. Maslovski, Comment on "Repulsive Casimir Force in Chiral Metamaterials", Phys. Rev. Lett. **105**, 189301 (2010).

[29] M. G. Silveirinha, Poynting vector, heating rate, and stored energy in structured materials: A first-principles derivation, Phys. Rev. B **80**, 235120 (2009).

[30] J. T Costa, M. G. Silveirinha, and A. Alù, Poynting vector in negative-index metamaterials, Phys. Rev. B **83**, 165120 (2011).

[31] M. G. Silveirinha and S. I. Maslovski, Exchange of Momentum between Moving Matter Induced by the Zero-Point Fluctuations of the Electromagnetic Field, Phys. Rev. A **86**, 042118 (2012).

[32] A. Raman and S. Fan, Photonic Band Structure of Dispersive Metamaterials Formulated as a Hermitian Eigenvalue Problem, Phys. Rev. Lett. **104**, 087401 (2010).

[33] T. A. Morgado, D. E. Fernandes, and M. G. Silveirinha, Analytical solution for the stopping power of the Cherenkov radiation in a uniaxial nanowire material, Photonics, **2**, 702 (2015).

[34] S. Wittekoek, T. J. A. Popma, J. M. Robertson, and P. F. Bongers, Magneto-optic spectra and the dielectric tensor elements of bismuth-substituted iron garnets at photon energies between 2.2-5.2 eV, Phys. Rev. B **12**, 2777 (1975).

[35] J. A. Bittencourt, *Fundamentals of Plasma Physics*, 3rd ed., Chap. 10 (Springer-Verlag, New York, 2010).

[36] G. W. Hanson, E. Forati, and M. G. Silveirinha, Modeling of spatially-dispersive wire media: Transport representation, comparison with natural materials, and additional boundary conditions, IEEE Trans. Antennas Propag. **60**, 4219 (2012).

[37] R. E. Camley, Nonreciprocal surface waves, Surf. Sci. Rep. **7**, 103 (1987).

[38] A. R. Davoyan and N. Engheta, Theory of Wave Propagation in Magnetized Near-Zero-Epsilon Metamaterials: Evidence for One-Way Photonic States and Magnetically Switched Transparency and Opacity, Phys. Rev. Lett. **111**, 257401 (2013).

[39] F. Abbasi, A. R Davoyan, and N. Engheta, One-way surface states due to nonreciprocal light-line crossing, New J. Phys. **17**, 063014 (2015).

[40] A. Davoyan and N. Engheta, Electrically controlled one-way photon flow in plasmonic nanostructures, Nature Comm. **5**, 5250 (2014).

[41] M. G. Silveirinha, Additional Boundary Conditions for Non-connected Wire Media, New. J. Phys. **11**, 113016 (2009).

[42] M. G. Silveirinha, Additional Boundary Condition for the Wire Medium, IEEE Trans. Antennas Propag. **54**, 1766 (2006).

[43] D. Colton and R. Kress, *Inverse Acoustic and Electromagnetic Scattering Theory*, Sec. 6.3 (Springer-Verlag, Berlin, 1998).